Research Paper

THEMED ISSUE: PLUTONS: Investigating the Relationship between Pluton Growth and Volcanism in the Central Andes

GEOSPHERE

GEOSPHERE; v. 14, no. 3

doi:10.1130/GES01495.1

12 figures; 6 tables; 2 supplemental files

CORRESPONDENCE: tmlopez@alaska.edu

CITATION: Lopez, T., Aguilera, F., Tassi, F., de Moor, J.M., Bobrowski, N., Aiuppa, A., Tamburello, G., Rizzo, A.L., Liuzzo, M., Viveiros, F., Cardellini, C., Silva, C., Fischer, T., Jean-Baptiste, P., Kazayaha, R., Hidalgo, S., Malowany, K., Lucic, G., Bagnato, E., Bergsson, B., Reath, K., Liotta, M., Carn, S., and Chiodini, G., 2018, New insights into the magmatic-hydrothermal system and volatile budget of Lastarria volcano, Chile: Integrated results from the 2014 IAVCEI CCVG 12th Volcanic Gas Workshop: Geosphere, v. 14, no. 3, p. 983–1007, doi:10.1130/GES01495.1.

Science Editor: Raymond M. Russo
Guest Associate Editor: Shanaka de Silva

Received 12 January 2017
Revision received 4 December 2017
Accepted 21 March 2018
Published online 7 May 2018

New insights into the magmatic-hydrothermal system and volatile budget of Lastarria volcano, Chile: Integrated results from the 2014 IAVCEI CCVG 12th Volcanic Gas Workshop

Taryn Lopez[1], Felipe Aguilera[2], Franco Tassi[3], J. Maarten de Moor[4], Nicole Bobrowski[5,6], Alessandro Aiuppa[7,8], Giancarlo Tamburello[9], Andrea L. Rizzo[8], Marco Liuzzo[8], Fátima Viveiros[10], Carlo Cardellini[11], Catarina Silva[10], Tobias Fischer[12], Philippe Jean-Baptiste[13], Ryunosuke Kazayaha[14], Silvana Hidalgo[15], Kalina Malowany[16], Gregor Lucic[16,*], Emanuela Bagnato[11], Baldur Bergsson[17], Kevin Reath[18], Marcello Liotta[8], Simon Carn[19], and Giovanni Chiodini[9]

[1]Geophysical Institute, University of Alaska Fairbanks, 903 Koyukuk Drive, Fairbanks, Alaska 99775, USA
[2]Departamento de Ciencias Geológicas, Universidad Católica del Norte, Avenida Angamos 0610, Antofagasta, Chile
[3]Department of Earth Sciences, University of Florence, Via G. La Pira 4, 50121 Florence, Italy
[4]Observatorio Vulcanológico y Sismológico de Costa Rica, Universidad Nacional, Heredia 40101, Costa Rica
[5]Institut für Geowissenschaften, Universität Mainz, Mainz 55099, Germany
[6]Institute for Environmental Physics, University of Heidelberg, Heidelberg 69047, Germany
[7]Dipartimento DiSTeM, Università di Palermo, Palermo 90123, Italy
[8]Istituto Nazionale di Geofisica e Vulcanologia (INGV), Sezione di Palermo, Via Ugo La Malfa 153, 90146 Palermo, Italy
[9]Istituto Nazionale di Geofisica e Vulcanologia, Sezione di Bologna, Bologna 40128, Italy
[10]Research Institute for Volcanology and Risk Assessment (IVAR), University of the Azores, Ponta Delgada 9500-321, Portugal
[11]Dipartimento di Fisica e Geologia, Università di Perugia, Via Pascoli snc, 06123 Perugia, Italy
[12]Department of Earth and Planetary Sciences, University of New Mexico, Albuquerque, New Mexico 87131, USA
[13]Laboratoire des Sciences du Climat et del'Environnement, CEA-CNRS-UVSQ, Centre de Saclay, 91191 Gif-sur-Yvette, France
[14]Magma Activity Research Group, Geological Survey of Japan, Tsukuba 305-8567, Japan
[15]Instituto Geofísico, Escuela Politécnica Nacional, Quito 170525, Ecuador
[16]Department of Earth and Planetary Sciences, McGill University, Montreal, Quebec H3A 0E8, Canada
[17]Icelandic Meteorological Office, Reykjavik 108, Iceland
[18]Department of Earth and Atmospheric Sciences, Cornell University, Ithaca, New York 14853, USA
[19]Department of Geological and Engineering Mining and Sciences, Michigan Technological University, Houghton, Michigan 49931, USA

ABSTRACT

Recent geophysical evidence for large-scale regional crustal inflation and localized crustal magma intrusion has made Lastarria volcano (northern Chile) the target of numerous geological, geophysical, and geochemical studies. The chemical composition of volcanic gases sampled during discrete campaigns from Lastarria volcano indicated a well-developed hydrothermal system from direct fumarole samples in A.D. 2006, 2008, and 2009, and shallow magma degassing using measurements from in situ plume sampling techniques in 2012. It is unclear if the differences in measured gas compositions and resulting interpretations were due to artifacts of the different sampling methods employed, short-term excursions from baseline due to localized changes in stress, or a systematic change in Lastarria's magmatic-hydrothermal system between 2009 and 2012. Integrated results from a two-day volcanic gas sampling and measurement campaign during the 2014 International Association of Volcanology and Chemistry of the Earth's Interior (IAVCEI) Commission on the Chemistry of Volcanic Gases (CCVG) 12th Gas Workshop are used here to compare and evaluate current gas sampling and measurement techniques, refine the existing subsurface models for Lastarria volcano, and provide new constraints on its magmatic-hydrothermal system and total degassing budget. While compositional differences among sampling methods are present, distinct compositional changes are observed, which if representative of long-term trends, indicate a change in Lastarria's overall magmatic-hydrothermal system. The composition of volcanic gases measured in 2014 contained high proportions of relatively magma- and water-soluble gases consistent with degassing of shallow magma, and in agreement with the 2012 gas composition. When compared with gas compositions measured in 2006–2009, higher relative H_2O/CO_2 ratios combined with lower relative CO_2/S_t and H_2O/S_t and stable HCl/St ratios (where S_t is total S [SO_2 + H_2S]) are observed in 2012 and 2014. These compositional changes suggest variations in the magmatic-hydrothermal system between 2009 and 2012, with possible scenarios to explain these trends including: (1) decompression-induced degassing due to magma ascent within the shallow crust; (2) crystallization-induced degassing of a stalled magma body; (3) depletion of the hydrothermal system

*Current address: Picarro Inc., 3105 Patrick Henry Drive, Santa Clara, California 95085, USA

due to heating, changes in local stress, and/or minimal precipitation; and/or (4) acidification of the hydrothermal system. These scenarios are evaluated and compared against the geophysical observations of continuous shallow inflation at ~8 km depth between 1997 and 2016, and near-surface (<1 km) inflation between 2000 and 2008, to further refine the existing subsurface models. Higher relative H_2O/CO_2 observed in 2012 and 2014 is not consistent with the depletion or acidification of a hydrothermal system, while all other observations are consistent with the four proposed models. Based on these observations, we find that scenarios 1 or 2 are the most likely to explain the geochemical and geophysical observations, and propose that targeted shallow interferometric synthetic-aperture radar (InSAR) studies could help discriminate between these two scenarios. Lastly, we use an average SO_2 flux of 604 ± 296 t/d measured on 22 November 2014, along with the average gas composition and diffuse soil CO_2 flux measurements, to estimate a total volatile flux from Lastarria volcano in 2014 of ~12,400 t/d, which is similar to previous estimates from 2012.

INTRODUCTION

The chemical and isotopic composition of volcanic gases can provide insights into subvolcanic conditions and specifically can be used to identify the presence of shallow magma and/or hydrothermal aquifers. These data can complement and refine geophysical models whose methods alone are unable to distinguish different types of crustal fluids responsible for seismic tomography anomalies and sources of crustal inflation. Discrete volcanic gas measurements collected at Lastarria volcano (northern Chile) found evidence for a well-developed hydrothermal system between May 2006 and June 2009 from direct fumarole samples (Aguilera et al., 2012), and shallow magma with minimal hydrothermal influence in November 2012 from in situ plume sampling techniques (Tamburello et al., 2014). These apparently discrepant findings could be attributed to: (1) spatial variability among the individual sampled fumaroles and the bulk plume composition; (2) mixing, dilution, and chemical processing (e.g., condensation of steam) of the volcanic gases with ambient air for the in situ measurements (Tamburello et al., 2014); (3) short-term excursions from baseline gas compositions due to localized changes in stress; and/or (4) a change in the volcanic-hydrothermal system between the two measurements periods, which can be attributed to both exogenous (e.g., precipitation, weather) and endogenous (e.g., volcanic, stress) changes (Zimmer et al., 2017). In November 2014, the International Association of Volcanology and Chemistry of the Earth's Interior (IAVCEI) Commission on the Chemistry of Volcanic Gases (CCVG) hosted its 12th volcanic gas workshop in Chile and conducted a two-day comprehensive volcanic gas sampling campaign at Lastarria volcano. The aims of these workshops are to test, compare, validate, and refine new and existing measurement and analysis techniques to accurately quantify and characterize volcanic degassing. The results from previous workshops were summarized by Giggenbach and Matsuo (1991) and Giggenbach et al. (2001). Here we present integrated results from this community-wide effort to provide a synoptic characterization of Lastarria's volcanic gas emissions. Specifically, in this manuscript we: (1) integrate and compare gas composition and flux measurements collected using a variety of gas measurement techniques; (2) use our volcanic gas measurement results to confirm a change in Lastarria's magmatic-hydrothermal system; and (3) calculate an updated total degassing budget using a combination of remote sensing, diffuse degassing, and in situ gas composition measurements.

VOLCANIC SETTING

Lastarria volcano (25.168°S, 68.507°W, 5706 m elevation) is located in South America's Central Volcanic Zone on the Chilean-Argentinian border, ~250 km southeast of Antofagasta, Chile (Fig. 1). It is part of the larger Lastarria–Cordón del Azufre complex, known colloquially as Lazufre. Within Lazufre, the Lastarria volcanic complex comprises three different volcanic structures including: (1) Negriales lava field, constituted by an andesitic-to-dacitic lava flow succession (400 ± 60 to 116 ± 26 ka); (2) Espolón Sur, consisting of andesitic lava flows (150 ± 50 ka); and (3) Lastarria *sensu stricto* (herein referred to as Lastarria volcano), a compound stratovolcano formed by successions of andesitic lava flows and domes, andesitic pyroclastic flows, and avalanche deposits, with

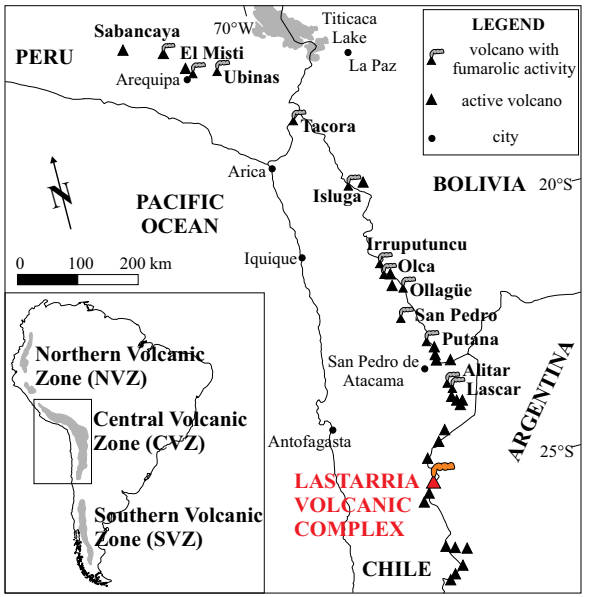

Figure 1. Regional map showing the location of the Lastarria volcanic complex, northern Chile. Modified from Aguilera et al. (2012).

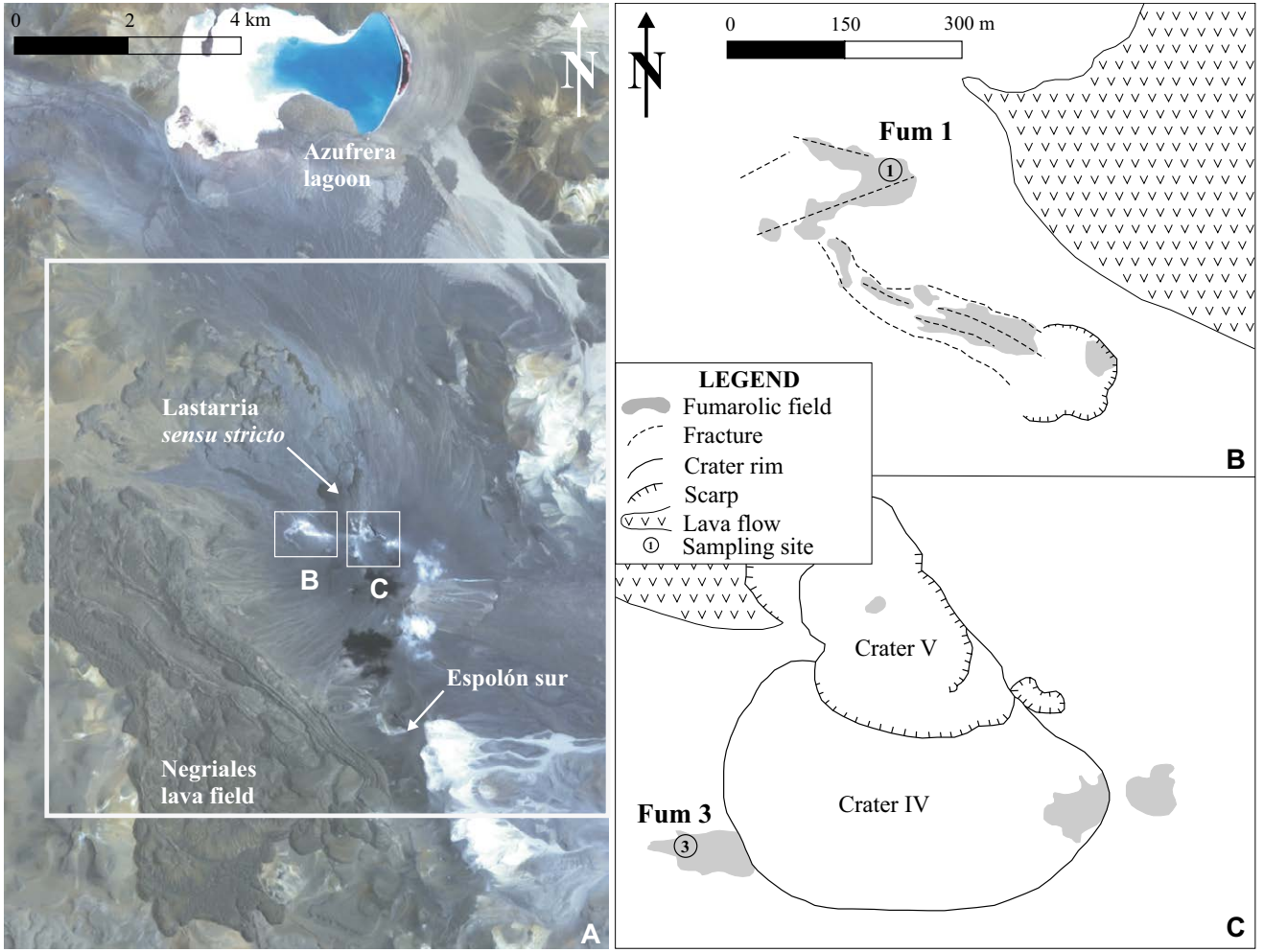

Figure 2. Advanced Spaceborne Thermal Emission and Reflection Radiometer (ASTER) image of the Lastarria volcanic complex (A), with the locations of the lower (B) and upper (C) fumarole fields (Fum 1 and Fum 3) marked by small white boxes; sketches of these regions shown on the right in B and C. The large white box shows the vertical and left-lateral extent of the region shown in Figure 3.

ages ranging from 260 ± 20 to <2.5 ka (Naranjo, 2010; Fig. 2). Lastarria volcano contains five overlapping summit craters and four actively degassing fumarole fields, two of which were measured in this study (Fig. 2). No historical eruptions from Lastarria volcano have been reported or observed, with its recent volcanic activity limited to persistent degassing, which was first observed in the early 19th century (González-Ferrán, 1995). However, Naranjo (2010) found evidence for profuse sulfur fumarolic activity prior to its 2.5 ka eruption, which continued after the eruption, forming the current four fumarolic fields and extensive sulfur flows.

Lastarria's edifice has been built on a basement of Pliocene- to Pleistocene-aged lavas from a diverse set of stratovolcanoes and lower Pleistocene dacitic ignimbrites (Naranjo and Puig, 1984; Naranjo and Cornejo, 1992; Naranjo, 2010). The continental crust in this region is estimated to be ~60–70 km thick (James, 1971). The earthquake foci defining the Benioff zone and indicating the

top of the subducting slab are located ~140 km beneath the volcanic complex (Barazangi and Isacks, 1976, 1979). These boundaries are used to estimate the mantle wedge thickness beneath Lastarria's crust at ~70–80 km.

PREVIOUS DEFORMATION AND GAS MEASUREMENTS

Large-scale crustal inflation centered between Lastarria and Cordón del Azufre was first detected by interferometric synthetic-aperture radar (InSAR) data beginning in ca. 1997–1998 (Pritchard and Simons, 2002) and has made this region the target of international multidisciplinary research (Pritchard et al., 2018). Following these initial findings, Froger et al. (2007) analyzed InSAR data collected between 2003 and 2005 and identified two inflation sources beneath Lastarria, including a deeper source located at 7–15 km depth and a shallow source ~1 km below the summit. They speculated that both sources were related, with the deeper source representing magmatic intrusion and the shallow source representing pressurization of a hydrothermal system (Froger et al., 2007). Ruch et al. (2009) similarly observed a shallow inflation source at a depth of ~1 km between 2000 and 2008. Continued inflation of the 7–15 km source has been observed through 2010 at an average rate of 3 cm/yr by Pearse and Lundgren (2013) and at a reduced rate of <1.5 cm/yr between 2011 and 2016 by Henderson et al. (2017). Updated geodetic modeling has redefined the deep inflation source as a shallowly dipping ~20 km × 30 km sill centered at 8 km depth (Pearse and Lundgren, 2013). No new deformation studies able to discriminate changes in the shallow inflation source have been conducted, such that it is currently not known if the shallow source has continued to inflate since 2008.

Aguilera et al. (2012) collected volcanic gas samples from Lastarria's main fumarole fields during campaigns in May 2006, March 2008, April 2009, and June 2009. Aguilera et al. (2012) then used the chemical composition and temperature of the volcanic gases, along with geochemical tools including geothermometers and isotopic tracers, to infer the presence of crustal magma degassing and a discontinuous shallow hydrothermal system. The geochemical interpretations of Aguilera et al. (2012) are consistent with the InSAR interpretations by Froger et al. (2007) indicating two deformation sources: a relatively deep magmatic source that is supplying the high-temperature magmatic gases, and a shallow boiling hydrothermal system within Lastarria's edifice that is supplying the low-temperature gas emissions. More recently, Spica et al. (2015) used high-resolution seismic tomography from data acquired during campaigns in 2008 and 2012 to identify two shallow low-velocity zones located at depths of <1 km and between 3 and 6 km centered beneath Lastarria's edifice. Spica et al. (2015) interpreted these low-velocity zones to represent the previously proposed shallow hydrothermal system and a potentially fluid-rich region overlying the ~8-km-depth magma source.

In November 2012, in situ plume composition and remote SO_2 flux measurements collected by Tamburello et al. (2014) indicated high fluxes of SO_2 and HCl gases consistent with shallow magma degassing and minimal hydrothermal scrubbing, in contrast to previous observations by Aguilera et al. (2012). Then between 2013 and 2015, Zimmer et al. (2017) collected continuous temperature, precipitation, and CO_2 measurements from three of Lastarria's high-temperature fumaroles to evaluate the influence of external processes on fumarole output. They found that major precipitation events caused significant temperature decreases at individual fumaroles over time scales of hours to days, but in most cases the fumarole then returned to its baseline temperature. They also found that changes in barometric pressure did not correlate with CO_2 output from high-temperature fumaroles.

Lastly, Carn et al. (2017) used temporal and spatial averaging techniques with Ozone Monitoring Instrument (OMI) satellite observations of SO_2 to calculate annual SO_2 emissions from Lastarria. These emissions ranged from 59 to 134 kt/yr between 2005 and 2015, and while some temporal variability in degassing is evident, the only temporal trend observed is a slight increase in SO_2 flux between 2010 and 2015.

METHODS

During the CCVG gas workshop, participants conducted a comprehensive volcanic gas sampling campaign at Lastarria volcano on 21 and 22 November 2014. These measurements were collected during optimal (clear sky) weather conditions within the dry season, with no major precipitation events having occurred in the previous weeks (Zimmer et al., 2017). The main objectives were to: (1) collect direct fumarole samples and in situ gas composition measurements from the summit and flank fumarole fields; and (2) measure volcanic outgassing of SO_2 and CO_2 using ground-based remote sensing and diffuse soil degassing techniques, respectively. Direct fumarole sampling and in situ plume measurements targeted fumaroles located in fields 1 and 3 as defined by Aguilera et al. (2012) (Figs. 2, 3), and referred to throughout this document as the lower (field 1) and upper (field 3) fields, respectively. The selected fumaroles correspond with the most representative high-temperature and high-flux fumaroles of the four fumarolic fields, and have exhibited notably stable temperatures and fluxes over time, based on previous work by Aguilera et al. (2012). Additionally, the lower and upper field fumaroles are the main contributors to the bulk plume and for that reason were targeted in this study. Diffuse soil degassing targeted the region around the lower field (Fig. 3). SO_2 camera measurements were collected north of the edifice to obtain a perpendicular view of the plume, while differential optical absorption spectroscopy (DOAS; Platt and Stutz, 2008) traverse measurements were collected downwind (east) of the edifice underneath the plume (Fig. 3).

Direct Fumarole Sampling

Direct fumarole samples for analysis of chemical and/or isotopic composition were collected by various teams including: University of New Mexico (USA; UNM); University of Florence (Italy; UNIFI); Istituto Nazionale di

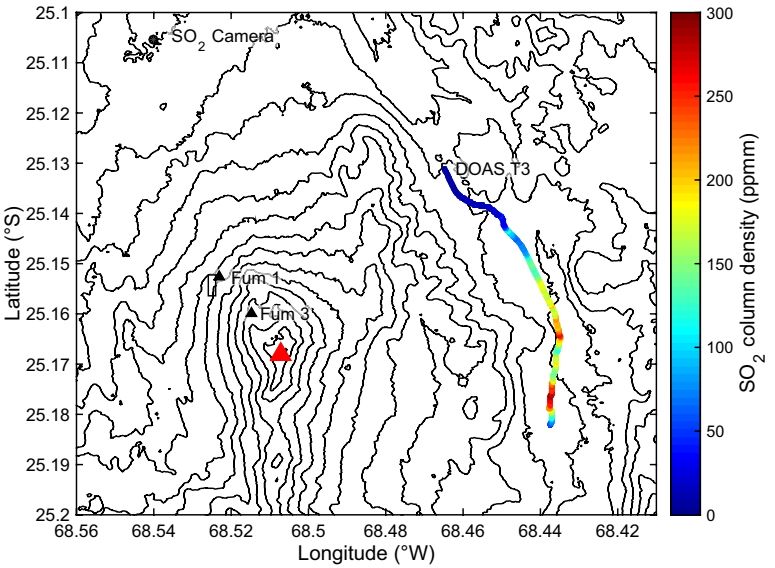

Figure 3. Location map of Lastarria volcano (red triangle), depicting the primary degassing and measurement sites including the upper (Fum 3) and lower (Fum 1) fumarole fields (black triangles), the SO_2 camera site (black circle), the diffuse degassing survey region (black rectangle), and location of an example differential optical absorption spectroscopy (DOAS) traverse (DOAST3) conducted in this study. The color bar represents the measured SO_2 column densities (ppmm [parts per million × meter]) observed during the third DOAS traverse on 22 November 2014, with two peaks in SO_2 likely reflecting degassing from the lower and upper fumarole fields. See text for details.

Geofisica e Vulcanologia Palermo (Italy; INGV-Palermo); Observatorio Vulcanológico y Sismológico de Costa Rica–Universidad Nacional (Costa Rica; UNA); French Atomic Energy Commission–Saclay (France; CEA); and McGill University (Canada; MU). A single fumarole from each field was targeted such that direct comparison of results from multiple groups would be possible. At each target fumarole, a 1-m-long, 2.5-cm-diameter titanium tube was inserted into the fumarolic vent and connected either through quartz Dewar tubes or through a glass adapter and Tygone and Silcone tubing to the sampling flasks. Traditional gas sampling techniques using pre-weighed evacuated bottles containing a caustic 4–5 N NaOH solution connected directly to the sampling line were used to quantify the major and trace element composition of fumarolic gases including H_2O, CO_2, SO_2, H_2S, HCl, HF, N_2, O_2, Ar, H_2, CH_4, CO, and He following the methods of Giggenbach and Goguel (1989). Additionally, the UNIFI group's bottles also contained 0.15 M $Cd(OH)_2$ to directly precipitate H_2S as CdS, enabling separate analyses of H_2S and SO_2 as described by Montegrossi et al. (2001). A total of six and three Giggenbach-style samples were collected from the lower and upper field fumaroles, respectively. With the exception of samples collected by INGV-Palermo on 22 November, all other Giggenbach samples were collected on 21 November. The MU group collected two fumarolic gas samples from the lower field on 21 November and four from the upper field on 22 November by syringe from the end of the sampling line and immediately transferred the sampled gas into evacuated bottles containing $HgCl_2$ (to prevent bacterial growth) for later analysis of CO_2 concentration and carbon isotope composition. Additionally, the INGV-Palermo group collected six dry gas samples from the lower field on 22 November by connecting a condensing system to the sampling line and allowing the gas to pass through the system prior to collection in two-stopcock bottles. The dry gas was sampled specifically to quantify He, H_2, O_2, N_2, CO, CH_4, and CO_2, as well as carbon isotope composition. Lastly, the group from CEA employed copper tubes connected to the sampling line to collect three dry-gas fumarolic gas samples from the lower field on 21 November for helium isotope analysis following the methods of Jean-Baptiste et al. (1992). Details of the various analytical methods employed are described in the following paragraphs.

Evacuated bottles containing absorbing (alkaline) solution were analyzed by each group in laboratories at UNM, UNIFI, UNA, and INGV-Palermo primarily following the methods of Giggenbach and Goguel (1989). Non-condensed (i.e., head-space) gases (e.g., N_2, O_2, CO, H_2, He, Ar, Ne, CH_4, and light hydrocarbons) were analyzed by gas chromatography. Absorbed gases including CO_2, total S ($S_t = SO_2 + H_2S$), HCl, and HF were quantified after oxidation and neutralization as dissolved SO_4^{2-}, Cl^-, and F^- by ion chromatography. Groups from UNM and UNIFI additionally quantified both SO_2 and H_2S in the alkaline solution following the methods of Giggenbach and Goguel (1989) and Vaselli et al. (2006), respectively. The H_2O content was determined by all groups by weighing the bottle before and after sampling, taking into account the amount of CO_2 and acidic species absorbed in alkaline solution. More details of the instruments and methods employed by individual groups can be found in Mitchell et al. (2010) and de Moor et al. (2013) (UNM and UNA), Vaselli et al. (2006) (UNIFI), and Sortino et al. (1991) (INGV-Palermo). The analytical uncertainties for acidimetric titration, gas chromatography, and ion chromatography are estimated at <10% for all groups.

All fumarolic measurements of $^{13}C/^{12}C$ are presented in comparison to the reference $^{13}C/^{12}C$ composition of Vienna Peedee belemnite (V-PDB; $^{13}C/^{12}C = 11{,}180.2 \times 10^{-6}$; Chang and Li, 1990) using standard delta notation. INGV-Palermo dry gas samples were analyzed by a Perkin Elmer Clarus 500 gas chromatograph equipped with a 3.5 m Carboxen 1000 column and double detector (hot-wire detector and flame ionization detector) with analytical errors <3%, while the carbon-isotope composition of CO_2 was measured using a dual-inlet mass spectrometer (Delta Plus, Finnigan), with an analytical uncertainty of ~0.1‰. The MU samples were analyzed in the geochemistry laboratory at MU in Montreal, Canada, on a Picarro G1101-i cavity ring-down spectrometer (CRDS). The standard deviation of the isotopic CO_2 values is <0.5‰. Additional details of the methods employed can be found in Lucic et al. (2015) and Malowany et al. (2015).

CEA samples for simultaneous helium and neon isotope determination were analyzed at the Saclay Nobel Gas Facility using a MAP215-50 mass spectrometer (Jean-Baptiste et al., 1992, 2010). The measured $^3He/^4He$ ratios (R) are

presented in comparison with the same ratio in air ($R_A = 1.39 \times 10^{-6}$; Mamyrin and Tolstikhin, 1984) as R/R_A. Typical ^4He and ^{20}Ne blanks were 5×10^{-10} and 3×10^{-10} cm^3, respectively (standard temperature and pressure), and analytical uncertainties on R/R_A and helium mixing ratios were ±0.05 and ±0.1 ppmv, respectively.

In Situ Plume Sampling (MultiGAS and Alkaline Trap)

Two types of in situ plume measurements were carried out by three groups at the upper and lower fumarole fields on 21 and 22 November including continuous, high-temporal-resolution major species gas composition (H_2O, CO_2, SO_2, H_2S) measurements using a multi-component gas analyzer system (MultiGAS), and average acid gas composition (S_t, HCl, HF, HBr) sampled over a discrete time period using alkaline trap methods.

MultiGAS measurements of major species plume composition were collected from the lower fumarole field by a group from the University of Palermo (Italy; UNIPA). The MultiGAS instrument contains a LICOR LI-840A infrared analyzer for simultaneously quantifying CO_2 and H_2O; and City Technology electrochemical sensors 3ST/F to quantify SO_2, EZ3H to quantify H_2S, and EZT3HYT to quantify H_2. Measurements were collected for ~2 h between 12:24 and 14:33 UTC on 22 November 2014 in "mobile" mode by UNIPA. During this time period, three transects were conducted while walking through the fumarole field. Molar gas ratios for the full data set were calculated by conducting linear interpolations of each measured gas species with respect to SO_2 over the sample period using RatioCalc software (Tamburello, 2015). No barometric pressure corrections were applied to the SO_2 and H_2S data due to the ineffectiveness of these corrections at high altitudes (Peter Kelly, 2017, personal commun.).

Two styles of alkaline trap sampling techniques were employed, both of which involve pulling plume air through an alkaline solution to absorb acid gases. Samples were collected on 21 November from the upper field and on 22 November from the lower field. The group from INGV-Palermo used Drechsel bottles containing ~100 ml of alkaline solution (1 M NaOH) and a pump to pull the volcanic gas–atmospheric mixture through the solution at a 1 L/min flow rate (e.g., Roberts and McKee, 1959; Liotta et al., 2012; Rizzo et al., 2013; Wittmer et al., 2014). This method enabled quantification of S_t and HCl. This sampling system was installed downwind of fumarolic gases in an area that appeared free of soil gas emissions. A group from the University of Heidelberg (UH) used a Raschig tube (e.g., Levin et al., 1980)–style alkaline trap made in house (see Wittmer et al., 2014), which was filled with 50 ml of a 1 M NaOH solution to enable quantification of S_t, HCl, HF, HBr, and HI. The volcanic gas–atmosphere mixture was pumped through the tube using a GilAir Plus pump (Sensidyne) set at a constant 4 L/min flow rate. Following collection, the samples collected by both the UH and INGV-Palermo teams were stored, prepared, and analyzed according to the methods of Wittmer et al. (2014) at laboratories within INGV-Palermo. All samples were analyzed using ion chromatography (Thermo Scientific Dionex ICS1100 and ICS5000) to quantify sulfur, chlorine, and fluorine content, and those of the UH group were also analyzed by inductively coupled plasma–mass spectrometry (ICP-MS; Agilent 7500 CE) to quantify the bromine and iodine content.

Remote Sensing

Two styles of ground-based remote sensing were employed during the field campaign to measure SO_2 column densities (ppmm [parts per million × meter]) across Lastarria's plume, allowing SO_2 and total volatile fluxes (t/d) to be calculated. These methods include: (1) stationary SO_2 camera measurements, and (2) zenith-looking DOAS traverse measurements (Fig. 3). Both methods utilize scattered solar radiation and the SO_2 absorption spectrum within the ultraviolet (UV) wavelength region to quantify the amount of SO_2 within an atmospheric column. On 21 November, SO_2 camera measurements were collected by a group from UNIPA, while walking traverse measurements were collected around the crater rim downwind of the upper field fumaroles by the UNA group. On 22 November, SO_2 camera measurements were repeated from the same site by groups from UNIPA and the Geological Survey of Japan (AIST), while vehicle-based DOAS traverses were conducted downwind of the plume on the east side of the edifice by groups from the Instituto Geofísico–Escuela Politécnica Nacional (Ecuador; IG-EPN) and the University of Alaska Fairbanks (UAF). More details of these measurements and their expected errors are described below.

SO_2 Camera

On 21 and 22 November, SO_2 camera measurements were collected from a location north of the edifice at a distance of ~7 km from the plume (Fig. 3) and with near-perpendicular views of the plume. On both days, the plume was hugging the ground such that SO_2 from the entire plume was not quantified and total calculated fluxes are likely underestimated. The group from AIST used an Apogee Alta F260 camera, while the group from UNIPA used a Jai CM-140GE camera. Both groups employed double camera systems with filters centered at 310 and 330 nm, to enable SO_2 column density to be quantified (Kern et al., 2015). Absorbance of UV radiation by SO_2 gas was converted to column densities using a combination of integrated DOAS measurements and calibration cells. Plume speed was calculated using the acquired plume imagery and feature tracking software (e.g., ImageJ with the MtrackJ plugin; Abràmoff et al., 2004; Taddeucci et al., 2012) to manually track the plume's main features.

On 21 November between 19:56 and 20:16 UTC, continuous SO_2 camera measurements of the bulk plume were collected by UNIPA at a 1 s sample rate. The light intensity data were corrected for light dilution effects (Mori et al., 2006; Kern et al., 2010) using the following procedure. First the reflectivity of a rock within the image field of view was assumed to be zero, and then the average measured UV intensity of the rock was subtracted from the 310 and

330 nm filtered data. On 22 November, continuous SO_2 camera measurements were collected by the AIST group between 14:01 and 14:16 UTC. Measured column densities were corrected for atmospheric dilution using a different procedure than described above. Specifically, coincident DOAS spectral data and SO_2 imagery were used following the methods of Campion et al. (2015) and Kazahaya et al. (2013) to calculate a range of light dilution causing the intensity data to be underestimated by ~50%–60%. The SO_2 fluxes were corrected to compensate for this underestimation. We note that on both days, a ground-hugging plume geometry and the transport of the lower field plume in front of the edifice prevented the entire plume from being measured from the SO_2 camera site, such that these fluxes may be underestimated by ~10%–30% based on visual observations. Considering this factor in addition to standard errors in SO_2 column density and plume speed, we estimate a total error in these calculated SO_2 fluxes to be ~50%.

DOAS Traverse

DOAS traverse measurements were made to quantify absorption of UV light by plume SO_2 gas by the UNA, IG-EPN, and UAF groups using Ocean Optics (S2000 and USB2000 model) spectrometers. SO_2 was calculated from the measured absorption spectra using clear (SO_2-free) sky and dark (instrument noise) spectra measured in the field, along with: (1) laboratory spectra of SO_2 and O_3, a Ring spectrum to account for inelastic (Raman) scattering, and a fifth-order polynomial to account for broadband extinction, through application of a spectral fitting routine integrated in NOVAC mobile DOAS software (Zhang and Johansson, 2009; Galle et al., 2010) (UNA and IG-EPN); and (2) field measurements of high- (1305 ppmm) and low-concentration (482 ppmm) calibration cell spectra integrated in a FLYSPEC system (Horton et al., 2006; Businger et al., 2015) (UAF). Spectral data were analyzed between ~310 and 325 nm (UNA and IG-EPN) and between 319 and 330 nm (UAF). In all cases, coincident GPS measurements were collected to obtain measurement time and location. Plume speed was estimated from windspeed using: (1) handheld anemometer measurements from the Lastarria crater rim at plume height by the UNA group, and (2) modeled wind data from the U.S. National Ocean and Atmospheric Administration (NOAA) for Lastarria's summit altitude and approximate sample collection time by the IG-EPN and UAF groups. In all cases, measured SO_2 column densities were integrated over the plume width and multiplied by plume speed to calculate SO_2 fluxes (t/d). The calculated standard error for the DOAS traverse measurements based on the error in the DOAS fit and windspeed is ~30%.

Two walking traverses on the upper field crater were made by UNA to measure SO_2 column densities and calculate SO_2 mass fluxes from the condensed upper field fumarolic plume on 21 November 2014 between 16:57 and 17:49 UTC. Then on 22 November, three vehicular-based DOAS traverses were conducted downwind and ~1 km beneath Lastarria's translucent plume by UAF and IG-EPN in the same vehicle between 14:09 and 15:24 UTC (Fig. 3).

Diffuse Soil Degassing

Soil CO_2 flux measurements were carried out at Lastarria on 21 November by groups from the Research Institute for Volcanology and Risk Assessment (University of the Azores, Portugal; IVAR) and the University of Perugia (Italy; UNIPE). A total of 139 measurements based on the accumulation chamber method (Chiodini et al., 1998) were made surrounding the lower fumarolic field (Fig. 3). Soil temperature at 15 cm depth was also recorded in 91 of the sampled sites. For reference purposes, six "background flux" measurements were performed ~5 km northwest of the lower fumarole field, near the SO_2 camera site (Fig. 3).

A soil CO_2 flux map was generated using the discrete soil CO_2 flux measurements made over an area of 38,725 m^2. The soil CO_2 flux and temperature maps were generated following the sequential Gaussian simulation (sGs) method (Deutsch and Journel, 1998; Cardellini et al., 2003). As the sGs method needs a multi-Gaussian distribution of the data, which implies a normal distribution of the values, original data were transformed into a normal distribution using the "nscore" algorithm by Deutsch and Journel (1998). Furthermore, the normality of the bivariate cumulative distribution function of any pairs of values, the second condition required by the multi-Gaussian model (Deutsch and Journel, 1998), was checked. Experimental variograms were computed and the derived variogram models were used in the sGs to create 100 realizations of the flux and temperatures grids (Supplemental Fig. S1[1]). The E-type estimate maps, i.e., the maps of the "expected" value at any location obtained through a pointwise linear average of all the realizations, are shown in Figure 4. The total CO_2 released by soil diffuse degassing was computed by multiplying the "expected" values of each grid cell by the cell surface.

RESULTS

Chemical and Isotopic Composition of Volcanic Gases

The total gas composition as measured using Giggenbach bottles from sampled fumaroles on both the upper and lower fields comprised primarily H_2O (87.3–96.4 mol%), CO_2 (2.0–9.12 mol%), SO_2 (0.69–1.50 mol%), H_2S (0.51–0.85 mol%), and HCl (0.15–0.54 mol%) (excluding one outlier thought to be contaminated during analysis) (Table 1). The atmospheric components Ar (2.78×10^{-5} to 5.4×10^{-4} mol%), and O_2 (0–0.024 mol%) composed a relatively minor proportion of the emitted gases in most samples, suggesting minimal air contamination. H_2, a common gas in moderate- to high-temperature volcanic and hydrothermal emissions, was present at relatively high abundance (0.0067–0.18 mol%). The reduced carbon species made up a relatively minor component of the gas emissions (~1.2×10^{-6} to 2.47×10^{-5} mol% CO, 1.9×10^{-5} to 2.2×10^{-4} mol% CH_4). The remaining gas species analyzed include HF (0.002–0.01 mol%), N_2 (0.028–0.19 mol%) and He (1.5×10^{-5} to 1.47×10^{-4} mol%) (Table 1).

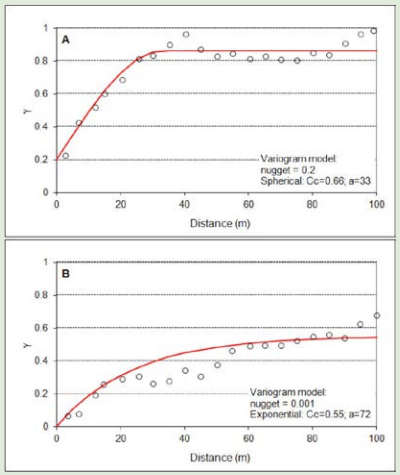

[1]Supplemental Figure S1. Omnidirectional variograms for soil CO_2 fluxes (A) and soil temperature (B) data. Please visit https://doi.org/10.1130/GES01495.S1 or the full-text article on www.gsapubs.org to view the Supplemental Figure.

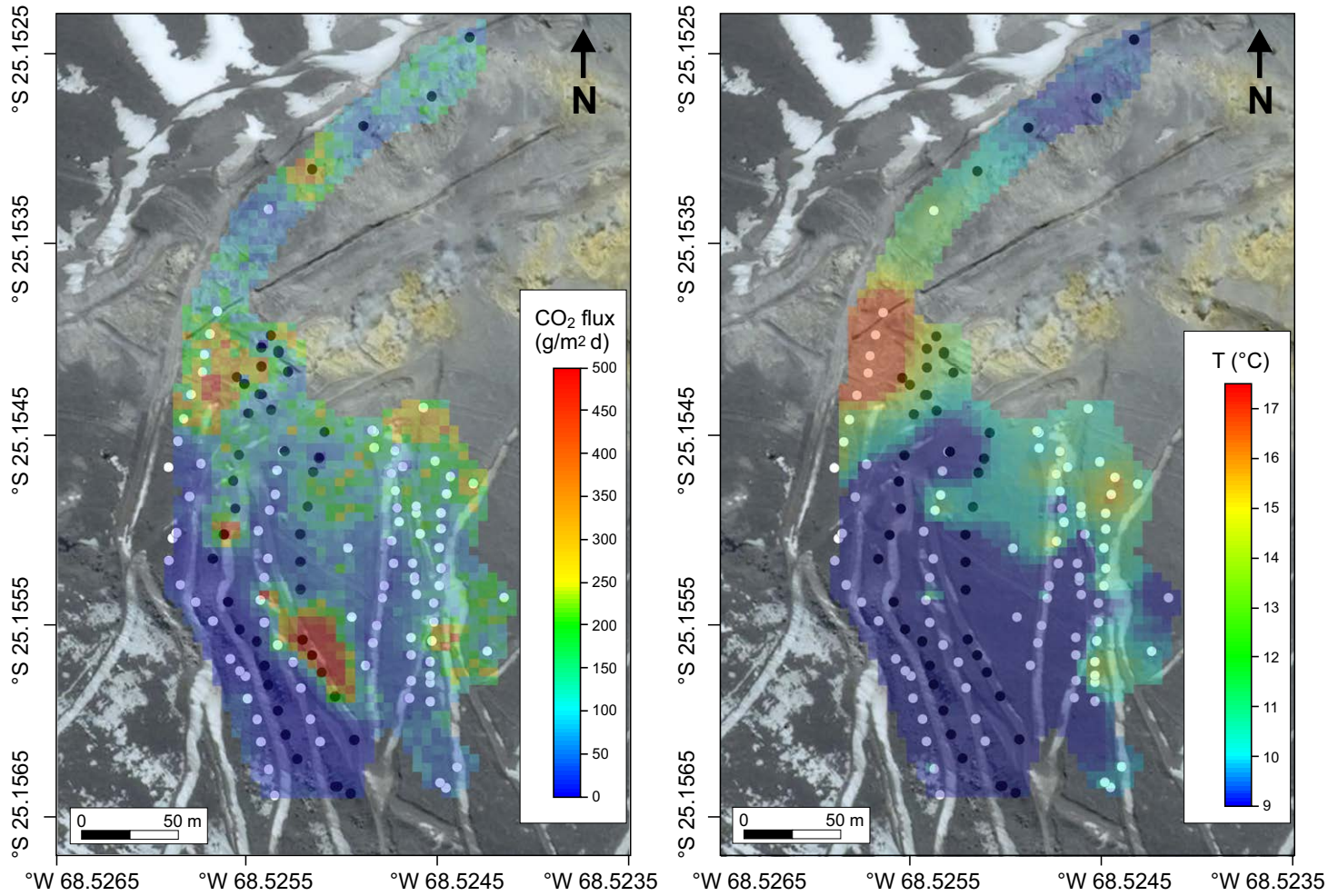

Figure 4. Soil measurements of diffuse CO_2 gas flux (left) and soil temperature (right) as measured from the lower fumarole field on 21 November 2014. White dots correspond to sampling sites where soil CO_2 flux and soil temperature were measured, and black dots represent sites where only soil CO_2 fluxes were measured. Base map 2016 Digital Globe, accessed via Google Earth on 9 December 2016 (http://earth.google.com). The location of the diffuse degassing survey region is shown in Figure 3 for regional context.

Good agreement was observed in $\delta^{13}C\text{-}CO_2$ between both upper and lower field fumaroles, and between the CRDS and mass spectroscopy analyses. All measurements converge around a mean value of –2.5‰ with a standard deviation of 0.3‰ (Table 2).

The Lastarria calculated R/R_A values from the three collected samples were highly similar, with a mean value of 5.12 and a standard deviation of 0.005. $^4He/^{20}Ne$ ratios (between 159.9 and 199.1) were used to correct for minor contamination by atmospheric air assuming a purely atmospheric origin for neon (Hilton, 1996). The resulting air-corrected mean R_c/R_A value is 5.13 with a measured helium concentration in the range of 11.9–13.3 ppm.

Major species gas mixing ratios (error ≤5%) measured by the MultiGAS from the lower fumarole field, representing emissions from numerous coalesced fumaroles (referred here as the plume), ranged from 400 to 800 ppm CO_2, 0.1 to 160 ppm SO_2, and 0.1 to 60 ppm H_2S. After subtracting local atmo-

TABLE 1. MEASURED TOTAL GAS COMPOSITION FROM LASTARRIA VOLCANO (NORTHERN CHILE) UPPER AND LOWER FUMAROLE FIELDS MEASURED BY GIGGENBACH BOTTLES DURING THIS STUDY

Sample name	Date	Temperature (°C)	H_2O (mol%)	CO_2 (mol%)	HCl (mol%)	HF (mol%)	SO_2 (mol%)	H_2S (mol%)	Total S (mol%)	N_2 (mol%)	CH_4 (mol%)	Ar (mol%)	O_2 (mol%)	H_2 (mol%)	He (mol%)	CO (mol%)	Collection team
Fumarole field 1 (lower field)																	
LAST_22112014_DG7_ALRML	22 Nov 2014	260	91.21	5.73	0.42	0.0067	nm	nm	2.24	0.193	4.14×10^{-5}	nm	0.0240	0.184	6.26×10^{-5}	1.83×10^{-6}	INGV-Palermo
LAST_22112014_DG8+_ALRML	22 Nov 2014	260	91.97	5.45	0.41	0.0098	nm	nm	2.07	0.028	1.88×10^{-5}	nm	bdl	0.0696	4.92×10^{-5}	1.77×10^{-6}	INGV-Palermo
LAST_11212014_DS2_LF_TF	21 Nov 2014	260	93.12	5.00	0.15	0.0051	1.03	0.61	1.64	0.069	3.41×10^{-5}	1.59×10^{-4}	3.40×10^{-6}	0.0185	1.47×10^{-4}	1.09×10^{-5}	UNM
LAST_11212014_DS2_LF_FT	21 Nov 2014	260	91.86	5.60	0.36	0.0074	1.20	0.85	2.05	0.0740	3.30×10^{-5}	3.80×10^{-4}	2.40×10^{-4}	0.0510	7.00×10^{-5}	1.20×10^{-6}	UNIFI
LAST_21112014_UNA9_LF_MdM	21 Nov 2014	260	90.94	6.45	0.36	0.0042	nm	nm	2.20	0.0438	2.24×10^{-5}	2.78×10^{-5}	5.16×10^{-4}	0.00672	1.50×10^{-5}	2.47×10^{-5}	UNA
LAST_21112014_UNA24_LF_MdM	21 Nov 2014	260	87.33	9.12	0.54	0.0056	nm	nm	2.83	0.0674	5.17×10^{-5}	9.42×10^{-5}	0.00153	0.104	2.26×10^{-5}	2.13×10^{-5}	UNA
Mean			**91.07**	**6.22**	**0.37**	**0.0064**	**1.12**	**0.73**	**2.17**	**0.0792**	$\mathbf{3.36 \times 10^{-5}}$	$\mathbf{1.65 \times 10^{-4}}$	**0.00438**	**0.07231**	$\mathbf{6.11 \times 10^{-5}}$	$\mathbf{1.03 \times 10^{-5}}$	
1σ standard deviation			2.0	1.5	0.13	0.0020	0.12	0.17	0.39	0.058	1.2×10^{-5}	1.5×10^{-4}	0.010	0.065	4.7×10^{-5}	1.1×10^{-5}	
Fumarole field 3 (upper field)																	
LAST_11212014_DS1_UF_TF	21 Nov 2014	180	96.39	2.00	0.27	0.012	0.69	0.51	1.20	0.0352	2.23×10^{-4}	1.18×10^{-4}	8.80×10^{-6}	0.089	1.26×10^{-4}	1.09×10^{-5}	UNM
LAST_11212014_DS1_UF_FT	21 Nov 2014	180	93.71	3.30	0.39	0.008	1.50	0.78	2.28	0.150	6.20×10^{-5}	5.40×10^{-4}	1.10×10^{-4}	0.160	8.00×10^{-5}	1.50×10^{-6}	UNIFI
LAST_21112014_UNA26_UF_MdM*	21 Nov 2014	180	90.88	3.30	2.62	0.017	2.77	nm	2.77	0.060	1.20×10^{-4}	1.76×10^{-4}	0.00251	0.357	1.45×10^{-5}	bdl	UNA
Mean			**95.05**	**2.65**	**0.33**	**0.010**	**1.10**	**0.65**	**1.74**	**0.093**	$\mathbf{1.42 \times 10^{-4}}$	$\mathbf{3.29 \times 10^{-4}}$	$\mathbf{5.94 \times 10^{-5}}$	**0.12**	$\mathbf{1.03 \times 10^{-4}}$	$\mathbf{6.20 \times 10^{-6}}$	
1σ standard deviation			1.9	0.92	0.085	0.0030	0.57	0.19	0.76	0.081	1.1×10^{-4}	2.9×10^{-4}	7.2×10^{-5}	0.050	3.2×10^{-5}	6.7×10^{-6}	

Abbreviations: nm—not measured; bdl—below detection limit; Total S—SO_2 + H_2S.
Collection team abbreviations: INGV—Istituto Nazionale di Geofisica e Vulcanologia (Italy), UNM—University of New Mexico (USA), UNIFI—University of Florence (Italy), UNA—Universidad Nacional Autonoma (Costa Rica).
*Sample thought to be contaminated with HCl in the laboratory and excluded from calculations.

spheric background for both H_2O and CO_2, the calculated molar gas ratios give H_2O/CO_2 of 6.2, CO_2/SO_2 of 2.2, and H_2S/SO_2 of 0.21. When gas composition is normalized to only include H_2O, CO_2, and S_t, a gas composition containing ~78.1 mol% H_2O, 12.7 mol% CO_2, and 9.1 mol% S_t is observed. Error in the molar gas ratios is estimated to be 20% based on experimental results of de Moor et al. (2016a).

The compositions from the two main degassing sites measured by alkaline traps were composed primarily of S_t (0.18–27.9 mmol/L) and HCl (0.21–5.48 mmol/L) (millimoles of the measured species per liter of air sampled), with minor quantities of HF (0.13–0.49 mmol/L), HBr (0.0022 mmol/L), and HI (0.003–0.007 mmol/L). Slightly lower relative HCl/S_t ratios were observed from the lower field emissions (HCl/S_t = 0.12–0.29) in comparison with the upper field (HCl/S_t = 0.20–0.47) (Table 3). Singular (Raschig tube) samples from each field were used to calculate an HF/S_t ratio of 0.009 and HBr/S_t of 1.5×10^{-4}.

Gas Fluxes

SO_2 Fluxes

On 21 November, plume speed from Lastarria's upper field crater was measured using a handheld anemometer at 14 m/s. These measurements were used along with the DOAS walking traverse measurements that day to calculate SO_2 fluxes from Lastarria's upper field only, ranging from 294 to 486 t/d, with an average value and 1σ standard deviation of 390 ± 136 t/d. SO_2 camera measurements by the UNIPA group acquired ~2 h later were used to calculate apparent plume speeds of 5 m/s based on feature tracking within the SO_2 imagery. The final SO_2 camera-derived fluxes for the bulk plume, corrected for light dilution, ranged from 417 to 916 t/d, with an average value and a 1σ standard deviation of 615 ± 87 t/d (Table 4).

On 22 November, AIST SO_2 camera measurements and feature tracking methods were used to calculate an average bulk plume speed of 9 m/s. After incorporating the light dilution correction, the final calculated AIST SO_2 camera fluxes between 14:01 and 14:16 UTC ranged from 664 to 1719 t/d with an average value and 1σ standard deviation of 1094 ± 193 t/d (Fig. 5). The expected error for these measurements is ~50%, resulting in a mean SO_2 flux and error range of 1094 ± 547. Plume speed was calculated for that same day by the UAF and IG-EPN groups using NOAA modeled wind data to be 9.7 m/s. Calculated SO_2 fluxes for UAF and IG-EPN, respectively, for the three traverses acquired between 14:09 and 15:24 UTC were: 759 and 903 t/d for traverse 1, 1033 and 997 t/d for traverse 2, and 1453 and 1334 t/d for traverse 3 (Fig. 5). The average flux and 1σ standard deviation for UAF and IG-EPN measurements respectively, were calculated to be 1082 ± 350 t/d (UAF) and 1078 ± 226 (IG-EPN)(Table 4). The upward-looking viewing geometry and closer distance to the plume minimizes errors due to light dilution and scattering (Mori et al., 2006; Kern et al., 2012), such that no corrections were done in these cases, and these measurements are assumed to be our most accurate. Then between 15:46 and 16:05 UTC, continuous SO_2 camera measurements were collected from the same SO_2 camera site (Fig. 5) by the UNIPA group. Plume speed for this time period was estimated to average 7 m/s based on plume

TABLE 2. ISOTOPIC GAS COMPOSITION AND VOLATILE SOURCE CALCULATIONS, LASTARRIA VOLCANO (NORTHERN CHILE)

Sample name	Fumarole field (field number)	Sample year	CO_2 (mol%)	$\delta^{13}C\text{-}CO_2$* (‰)	He (mol%)	R/R_A†	He/Ne	R_c/R_A§	^3He (mol%)	$CO_2/^3He$	M# (%)	C** (%)	O†† (%)	Reference
Dry gas samples for noble gas analyses														
LAST_21112014_DG1_GLKM	Lower (1)	2014	67.5	–2.91	–	NA	NA	–	–	–	–	–	–	This study, MU
LAST_21112014_DG2_GLKM	Lower (1)	2014	38.3	–2.95	–	NA	NA	–	–	–	–	–	–	This study, MU
LAST_22112014_DG3_GLKM	Upper (3)	2014	71.2	–1.95	–	NA	NA	–	–	–	–	–	–	This study, MU
LAST_22112014_DG4_GLKM	Upper (3)	2014	74.2	–2.29	–	NA	NA	–	–	–	–	–	–	This study, MU
LAST_22112014_DG5_GLKM	Upper (3)	2014	63.5	–2.43	–	NA	NA	–	–	–	–	–	–	This study, MU
LAST_22112014_DG6_GLKM	Upper (3)	2014	53.4	–1.99	–	NA	NA	–	–	–	–	–	–	This study, MU
LAST_22112014_DG1_ALRML	Lower (1)	2014	25.7	–2.58	–	NA	NA	–	–	–	–	–	–	This study, MU
LAST_22112014_DG2_ALRML	Lower (1)	2014	22.4	–2.37	–	NA	NA	–	–	–	–	–	–	This study, INGV-Palermo
LAST_22112014_DG3_ALRML	Lower (1)	2014	70.7	–2.93	–	NA	NA	–	–	–	–	–	–	This study, INGV-Palermo
LAST_22112014_DG4_ALRML	Lower (1)	2014	76.9	–2.43	–	NA	NA	–	–	–	–	–	–	This study, INGV-Palermo
LAST_22112014_DG5_ALRML	Lower (1)	2014	75.2	–2.57	–	NA	NA	–	–	–	–	–	–	This study, INGV-Palermo
LAST_22112014_DG6_ALRML	Lower (1)	2014	80.9	–2.44	–	NA	NA	–	–	–	–	–	–	This study, INGV-Palermo
Average $\delta^{13}C\text{-}CO_2$, 2014			**60.0**	**–2.49**	–	**NA**	**NA**	–	–	–	–	–	–	**This study**
LAST_21112014_DG1_PJB	Lower (1)	2014	–	–	–	5.13	0.060	5.14	–	–	–	–	–	This study, CEA-Saclay
LAST_21112014_DG2_PJB	Lower (1)	2014	–	–	–	5.12	0.077	5.13	–	–	–	–	–	This study, CEA-Saclay
LAST_21112014_DG3_PJB	Lower (1)	2014	–	–	–	5.12	0.083	5.13	–	–	–	–	–	This study, CEA-Saclay
Average helium, 2014			–	–	–	**5.12**	**0.073**	**5.13**						**This study, CEA-Saclay**
Combined CO_2 and He compositions, 2014§§			**5.1**	**–2.49**	**6.5×10^{-5}**	**5.12**	**0.073**	**5.13**	**4.6×10^{-10}**	**2.2×10^{10}**	**7**	**87**	**6**	**This study**
Volatile source calculations from previous work														
LSTG-12	Lower (1)	2008	94.7	–2.77	0.00021	NA	NA	5.4	1.6×10^{-9}	6.0×10^{10}	2	89	9	Aguilera et al., 2012
LSTG-16	Lower (1)	2009	94.6	–2.22	0.00036	NA	NA	5.8	2.9×10^{-9}	3.3×10^{10}	5	89	6	Aguilera et al., 2012
LSTG-18	Lower (1)	2009	91.6	–1.82	0.00023	NA	NA	6.2	2.0×10^{-9}	4.6×10^{10}	3	91	5	Aguilera et al., 2012
LSTB-21	Upper (3)	2006	95.2	–1.55	0.00071	NA	NA	4.9	4.9×10^{-9}	2.0×10^{10}	7	89	4	Aguilera et al., 2012
LSTG-27	Upper (3)	2009	92.3	–2.14	0.00018	NA	NA	6.2	1.6×10^{-9}	5.9×10^{10}	3	91	7	Aguilera et al., 2012

*$\delta^{13}C\text{-}CO_2$—isotopic composition of carbon on the CO_2 molecule is presented in standard delta notation [(R_s / R_{std} -1) × 1000], where R_s = $^{13}C/^{12}C$ of the sample and R_{std} = $^{13}C/^{12}C$ of the reference standard. The $^{13}C/^{12}C$ reference standard Vienna Peedee belemnite (V-PDB) has a value of $11{,}180.2 \times 10^{-6}$ (Chang and Li, 1990).

†The ratios of $^3He/^4He$ of the samples (R) are presented in comparison with the same ratio for the reference standard air (R_A).

§R_c represents the $^3He/^4He$ ratio of the samples after being corrected for air following the methods of Hilton (1996). R_A has a value of 1.39×10^{-6} (Mamyrin and Tolstikhin, 1984).

#Percent of C and He within the measured gases presumed to be sourced from the mantle (M) as calculated using the three-component mixing model of Sano and Marty (1995).

**Percent of C and He within the measured gases presumed to be sourced from (subducted or crustal) carbonates (C) as calculated using the three-component mixing model of Sano and Marty (1995).

††Percent of C and He within the measured gases presumed to be sourced from (subducted or crustal) organic matter (O) as calculated using the three-component mixing model of Sano and Marty (1995).

§§This row includes the average dry-gas $\delta^{13}C\text{-}CO_2$ and ^3He compositions from 2014 (above) combined with the average measured He and CO_2 wet-gas compositions from direct samples collected in 2014 from Table 1.

Reference column abbreviations: MU—McGill University (Canada); INGV—Istituto Nazionale de Geofisica e Vulcanologia (Italy); CEA—French Atomic Energy Commission (France).

Notes: Cells containing only dash mean that analyses or calculations were not conducted on these samples. NA—not available.

feature tracking of the SO_2 imagery. Following the light intensity correction, the calculated SO_2 fluxes ranged from 170 to 765 t/d, with an average value of 455 ± 90 t/d. The mean SO_2 flux (±1σ standard deviation) calculated by combining the traverse and SO_2 camera measurements on 22 November yields a value of 604 ± 296 t/d.

Diffuse Soil CO_2 Fluxes

The CO_2 released from Latarria's edifice as measured during the discrete soil degassing survey on 21 November was calculated by integrating the average CO_2 flux values estimated from sGs over the measurement area (~38,725 m²). These analyses yield a combined diffuse CO_2 flux of ~5 t/d. Dividing the calculated CO_2 output by the measurement area gives an average degassing flux from the sample region of 1.29×10^{-4} t/d/m².

DISCUSSION

Comparison of Gas Composition and Flux Measurements

Throughout this study, a variety of gas sampling and/or remote sensing measurements were employed to quantify the composition and flux of volcanic gases from Lastarria volcano. As previously mentioned, inherent differ-

TABLE 3. MEASURED GAS RATIOS AND CALCULATED AVERAGES FROM 2014 DIRECT SAMPLING, MULTIGAS, AND ALKALINE TRAP MEASUREMENTS, LASTARRIA VOLCANO (NORTHERN CHILE)

Sample name	Temperature (°C)	H_2O/CO_2	H_2O/S_t	CO_2/S_t	HCl/S_t	HF/S_t	HBr/S_t	Method	Collection team
Direct samples, lower field									
LAST_22112014_DG7_ALRML	260	16	41	2.6	0.19	0.0030	–	Direct sample	INGV-Palermo
LAST_22112014_DG8+_ALRML	260	17	44	2.6	0.20	0.0047	–	Direct sample	INGV-Palermo
Last_11212014_DS2_LF_TF	260	19	57	3.0	0.09	0.0031	–	Direct sample	UNM
Last_11212014_DS2_LF_FT	260	16	45	2.7	0.18	0.0036	–	Direct sample	UNIFI
LAST_21112014_UNA9_LF_MdM	260	14	41	2.9	0.16	0.0019	–	Direct sample	UNA
LAST_21112014_UNA24_LF_MdM	260	10	31	3.2	0.19	0.0020	–	Direct sample	UNA
Average direct sample, lower field	**260**	**15 ± 3**	**43 ± 8**	**2.9 ± 0.3**	**0.17 ± 0.04**	**0.0030 ± 0.001**	–	**Direct sample**	
MultiGAS measurements, lower field									
LAST_22112014_MG1_AA	–	6.3	13.2	2.1	–	–	–	MultiGAS	UNIPA
LAST_22112014_MG2_AA	–	6.8	11.3	1.70	–	–	–	MultiGAS	UNIPA
LAST_22112014_MG3_AA	–	5.4	8.8	1.60	–	–	–	MultiGAS	UNIPA
Average MultiGAS, lower field	–	**6.2 ± 0.7**	**11.1 ± 2.2**	**1.80 ± 0.3**	–	–	–	**MultiGAS**	**UNIPA**
Alkaline trap samples, lower field									
LAST_22112014_AT1_NB	–	–	–	–	0.20	0.010	1.0×10^{-4}	Alkaline trap	UH
LAST_22112014_AT1_ALRML	–	–	–	–	0.12	–	–	Alkaline trap	INGV-Palermo
LAST_22112014_AT2_ALRML	–	–	–	–	0.22	–	–	Alkaline trap	INGV-Palermo
LAST_22112014_AT3_ALRML	–	–	–	–	0.29	–	–	Alkaline trap	INGV-Palermo
Average alkaline trap, lower field	–	–	–	–	**0.21 ± 0.07**	**0.010**	**1.0×10^{-4}**	**Alkaline trap**	
Direct samples, upper field									
Last_11212014_DS1_UF_TF	180	48	80	1.7	0.23	0.010	–	Direct sample	UNM
Last_11212014_DS1_UF_FT	180	28	62	2.2	0.17	0.0036	–	Direct sample	UNIFI
LAST_21112014_UNA26_UF_MdM*	180	28	33	1.2	0.95	0.0063	–	Direct sample	UNA
Average direct sample, upper field	**180**	**38 ± 14**	**71 ± 13**	**1.9 ± 0.38**	**0.20 ± 0.038**	**0.0069 ± 0.0048**	–	**Direct sample**	
Alkaline trap samples, upper field									
LAST_21112014_AT1_NB	–	–	–	–	0.20	0.0088	1.5×10^{-4}	Alkaline trap	UH
LAST_21112014_AT1_ALRML	–	–	–	–	0.43	–	–	Alkaline trap	INGV-Palermo
LAST_21112014_AT2_ALRML	–	–	–	–	0.47	–	–	Alkaline trap	INGV-Palermo
LAST_21112014_AT3_ALRML	–	–	–	–	–	–	–	Alkaline trap	INGV-Palermo
Average alkaline trap, upper field	–	–	–	–	**0.37 ± 0.14**	**0.0088**	**1.5×10^{-4}**	**Alkaline trap**	
Average, all measurements	–	**17**	**40**	**2.4**	**0.17**	**0.0040**	**1.3×10^{-4}**	**All**	

*This sample is thought to be contaminated by HCl and is excluded from analysis.
Abbreviations: St—$SO_2 + H_2S$; MultiGAS—Multicomponent Gas Analyzer System; dashes indicate that samples/measurements were not collected or analyzed.
Collection team abbreviations: INGV—Istituto Nazionale di Geofisica e Vulcanologia (Italy); UNM—University of New Mexico (USA); UNA—Universidad Nacional Autonoma (Costa Rica); UNIFI—University of Florence (Italy); UNIPA—University of Palermo (Italy); UH—University of Heidelberg (Germany).

ences in the individual sampling methods prevent direct comparison of these data sets. Specifically, fumarole sample composition collected at a single emission source will differ from the bulk plume composition (a mixture of volcanic gases from numerous fumaroles and air) measured using in situ techniques such as MultiGAS and/or alkaline traps. While acknowledging these differences, we briefly compare complementary measurements and discuss in general variations among the data sets to better evaluate the limitations in our results and implications for our data interpretations.

Comparison of Gas Composition Measurements

In general, fairly good agreement in direct fumarole sample gas analysis collected in Giggenbach bottles was observed for measurements collected by various groups from the same fumarole (Tables 1 and 3). When normalized gas concentrations from Table 1 are evaluated, variations in individual gas species that, at times, exceed the analytical uncertainties (<10%) are observed. Variations in measured gas compositions from the same fumarole have been

TABLE 4. SUMMARY OF SO_2 FLUX MEASUREMENT PARAMETERS AND RESULTS, LASTARRIA VOLCANO (NORTHERN CHILE)

Measurement type	Team	Date (UTC)	Start time (UTC)	End time (UTC)	Number of measurements	Wavelength region (nm)	Viewing geometry	Distance from plume (km)	Plume appearance	Correction applied?	Plume speed (m/s)	Minimum SO_2 flux (t/d)	Maximum SO_2 flux (t/d)	Mean SO_2 flux (t/d)	Standard deviation (t/d)	Error (%)	Notes
DOAS walking traverse	UNA	21 November 2014	16:57	17:49	2	310–325	Zenith	<<1	Condensed	No	14	294	486	390	136	30	Fumarole field 3 only
SO_2 camera	UNIPA	21 November 2014	19:56	20:15	288	310, 330	Slant	7	Transparent	Yes—dilution	5	417	916	615	87	50	Grounded plume—only seeing 70%–90% of plume
SO_2 camera	AIST	22 November 2014	14:01	14:16	972	310, 330	Slant	7	Transparent	Yes—dilution	9	664	1719	1094	193	50	Grounded plume—only seeing 70%–90% of plume
DOAS vehicle traverse	UAF	22 November 2014	14:09	15:24	3	319–330	Zenith	1	Transparent	No	9.7	759	1453	1082	350	30	Optimal viewing conditions
DOAS vehicle traverse	IG-EPN	22 November 2014	14:10	15:20	3	310–325	Zenith	1	Transparent	No	9.7	903	1334	1078	226	30	Optimal viewing conditions
SO_2 camera	UNIPA	22 November 2014	15:46	16:05	969	310, 330	Slant	7	Transparent	Yes—dilution	7	170	764	455	90	50	Grounded plume—only seeing 70%–90% of plume

Abbreviations: DOAS—Differential Optical Absorption Spectroscopy. UNA—Universidad Nacional Autonoma (Costa Rica); UNIPA—University of Palermo (Italy); AIST—Geological Survey of Japan (Japan); UAF—University of Alaska Fairbanks (USA), IG-EPN—Instituto Geofisico - Escuela Politecnica Nacional (Ecuador).

Note: Correction applied refers to the dilution correction applied to SO_2 camera data to correct for the dilution of the SO_2 signal by SO_2-free air. See text for details of these correction methods.

observed at previous CCVG gas workshops, and mechanisms to account for these variations have been described in detail by Giggenbach and Matsuo (1991) and Giggenbach et al. (2001). The main factors contributing to these differences include: (1) variations in samples due to condensation or entrainment of water in the sample line and/or the outgassing itself, and (2) variations in analytical methods (Giggenbach et al., 2001). In particular, we note that variations in sulfur content and speciation (Tables 1 and 3) between groups from UNIFI and UNM are likely due to the different analytical methods employed (e.g., Vaselli et al., 2006; Giggenbach and Goguel, 1989). Because slight differences in the concentration of one measured gas species can have large effects on the normalized composition, we consider evaluation of gas ratios to be more useful for comparison purposes. When major species gas ratios determined by the various groups for the lower field fumarole samples are compared, we find good agreement, with the following average ratios and 1σ standard deviations found: $H_2O/CO_2 = 15 \pm 3$, $H_2O/S_t = 43 \pm 8$, $CO_2/S_t = 2.9 \pm 0.3$, and $HCl/S_t = 0.17 \pm 0.04$ (Table 3). When we consider the major species gas ratios directly sampled from the lower-temperature upper field fumarole, we find somewhat larger variations with the following average ratios and 1σ standard deviations: $H_2O/CO_2 = 38 \pm 14$, $H_2O/S_t = 71 \pm 13$, $CO_2/S_t = 1.9 \pm 0.38$, and $HCl/S_t = 0.20 \pm 0.04$ (Table 3). While variations in gas composition among the different sample collection groups can most likely be attributed to differences in sampling and analytical techniques (Table 1), general trends in gas composition can be identified to characterize the overall gas source. When the major species gas ratios for the lower and upper fumaroles are compared, the upper field fumarole appears to be enriched in H_2O, SO_2, and HCl relative to the lower field, which is relatively enriched in CO_2 (Table 3).

We next compare the average major species gas ratios measured by the MultiGAS to those measured through direct fumarole sampling from the lower

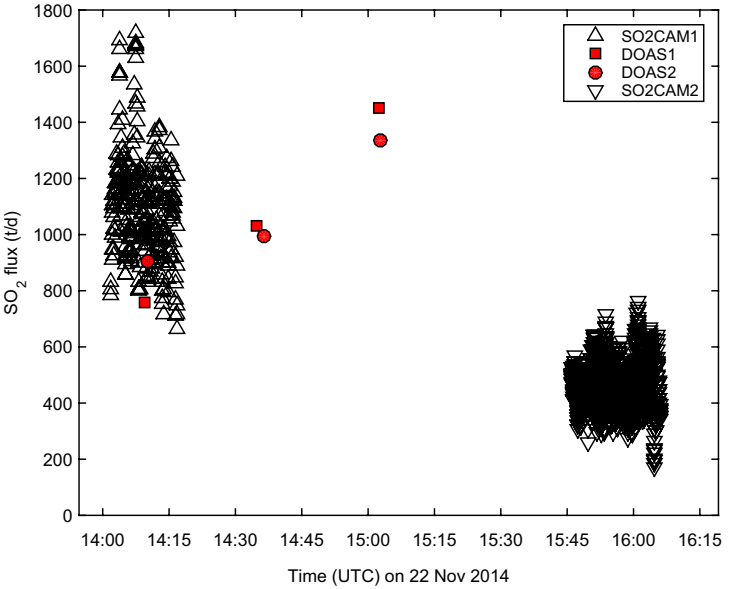

Figure 5. SO_2 mass fluxes (t/d) calculated from SO_2 camera and differential optical absorption spectroscopy (DOAS) traverse measurements of Lastarria volcano's plume on 22 November 2014. SO2CAM1 and SO2CAM2 represent SO_2 camera measurements made by the Geological Survey of Japan (AIST) and University of Palermo (Italy; UNIPA) groups, respectively, while DOAS1 and DOAS2 represent traverse measurements made by the University of Alaska Fairbanks (USA; UAF) and Instituto Geofísico–Escuela Politécnica Nacional (Ecuador; IG-EPN) groups, respectively. Assumed error bars of 50% for SO_2 camera data and 30% for DOAS traverses are not shown for clarity.

field. The average MultiGAS ratios observed of H_2O/CO_2 = 6.2 ± 0.7, H_2O/S_t = 11.1 ± 2.2, and CO_2/S_t = 1.8 ± 0.3 are all notably lower than the average observed ratios measured by direct fumarole sampling from the lower field (H_2O/CO_2 = 15 ± 3, H_2O/S_t = 43 ± 8, and CO_2/S_t = 2.9 ± 0.3), which can be explained in part through a relative depletion in H_2O compared to other gases for the bulk plume measured by the MultiGAS (Table 3). The observation of lower H_2O/CO_2 in MultiGAS measurements compared to direct fumarole samples has been previously observed in other volcanic gas studies, and has been attributed to condensation of water vapor in the plume before reaching the instrument (e.g., Allard et al., 2014; Lopez et al., 2017). In this case, a similar (e.g., Allard et al., 2014) or slightly higher CO_2/S_t ratio would be expected in the MultiGAS data compared to the fumarole sample compositions as depletion of H_2O due to condensation may also involve some absorption of SO_2 by water vapor. At Lastarria, however, depletions in both H_2O/CO_2 and CO_2/S_t are observed in the MultiGAS data relative to the fumarole samples, consistent with a higher proportion of sulfur gas measured by the MultiGAS. To explain this observation, we therefore conclude that at least two processes must be contributing to the variations in gas composition observed by the MultiGAS versus direct fumarole samples. Because the direct fumarole samples represent gases emitted from a single point source, while the MultiGAS measurements represent the composition of the bulk plume, it is likely that spatial heterogeneities in gas composition within the fumarole field may be partially contributing to these observed differences (e.g., Tamburello et al., 2015). We speculate that the MultiGAS measurements of CO_2/S_t may better represent Lastarria's bulk plume composition, including the highest-temperature, SO_2-rich fumaroles, as fumarole temperature and SO_2 composition are found to directly correlate (e.g., Aiuppa et al., 2005; Aguilera et al., 2012; Tamburello et al., 2015). We further speculate that the direct fumarole analyses of H_2O/CO_2 composition may best represent Lastarria's gas composition that has not been modified by steam condensation. We propose that future CCVG workshops conduct more detailed spatial sampling of fumarole fields by both MultiGAS and direct fumarole sampling methods to further constrain the differences between direct sampling and in situ gas measurements.

When the alkaline trap results are compared among the two collection groups, fair agreement in HCl/S_t was observed between the two sampling methods employed, with mean and 1σ standard deviations of 0.21 ± 0.07 and 0.37 ± 0.14 for the upper and lower fields, respectively (Table 3). The HCl/S_t ratios derived from the alkaline trap methods agree fairly well with those calculated from the direct fumarole sampling, with the alkaline trap measurements having consistently higher HCl/S_t (Table 3).

Comparison of SO_2 Flux Measurements

Variations in calculated SO_2 fluxes from Lastarria volcano that are within the assumed error are observed both within sampling periods by individual groups, as well as when measurements among the different groups are directly compared. Our results suggest fairly good agreement among the measurement techniques and somewhat consistent degassing over the study period. Unfortunately, the relatively large errors due in part to the ground-hugging plume geometry, which has increased the error in UV camera measurements to ~50%, do not enable us to discriminate potential volcanogenic variations in gas fluxes that have been observed at other volcanoes (e.g., Tamburello et al., 2013).

On 21 November, UNA DOAS traverse measurements from the upper field were collected 2 h prior to UV camera measurements by UNIPA. The DOAS traverse measurements yielded an average SO_2 flux of 390 ± 136 t/d, while the SO_2 camera results of the bulk plume yielded an average flux of 615 ± 87 t/d (Table 4). The condensed nature of the plume during walking traverses, which likely increased the occurrence of multiple scattering, suggests that these DOAS SO_2 fluxes may be overestimated (e.g., Kern et al., 2010). Similarly, the ground-hugging plume geometry likely resulted in underestimated SO_2 fluxes from the SO_2 camera. Using these measurements, we calculate that <60% of the total SO_2 flux may have been supplied by the upper field fumaroles, however due to the limitations described above, we expect that the actual proportion of SO_2 supplied by the upper field is quite a bit lower.

On 22 November, SO_2 camera measurements by AIST temporally overlap with a single DOAS traverse made by UAF and IG-EPN at ~14:10 UTC (Fig. 5). The most optimal viewing conditions (e.g., Kern et al., 2012) were experienced during these DOAS traverses as characterized by the translucent plume, vertical viewing geometry, and close location to the plume (estimated at <1 km), such that we expect these flux measurements to be the most accurate. Good agreement, well within the measurement error, was observed between the two groups conducting simultaneous DOAS traverse measurement for the three traverses conducted, with average and 1σ standard deviations of 1082 ± 350 by UAF and 1078 ± 226 by IG-EPN (Table 4; Fig. 5). We expect that the slight variations between the calculated fluxes were due to differences in SO_2 retrieval algorithms. This traverse, which took ~20 min to complete, was coincident with 6 min of AIST 1 Hz SO_2 camera measurements. During the overlapping time period, the minimum, maximum, and mean SO_2 camera–derived fluxes were 664, 1384, and 1038 t/d (Fig. 5). The mean SO_2 flux and 1σ standard deviation calculated by the three groups of 1082 ± 350 (UAF), 1078 ± 226 (IG-EPN), and 1038 ± 161 (AIST) are in excellent agreement.

Comparison with Previous Studies and Implications for Changes in Lastarria's Magmatic-Hydrothermal System

To accurately identify the temporal evolution of Lastarria's magmatic-hydrothermal system, continuous measurements of Lastarria's bulk plume composition over an extended time period are needed. Unfortunately, this and previous ground-based studies are limited to temporally discrete gas composition measurements from a select number of fumaroles or the bulk plume (Aguilera et al., 2012; Tamburello et al., 2014), and to continuous measurements of a single gas species (CO_2 and SO_2) from either a discrete number of

fumaroles (Zimmer et al., 2017) or the bulk plume averaged over a year-long period (Carn et al., 2017), which limits the interpretations that can be made. The longest time-series data set for Lastarria's gas emissions comes from temporally and spatially averaged OMI satellite SO_2 detections averaged over year-long periods between 2005 and 2015 (Carn et al., 2017). During this time, SO_2 emissions were persistently detectable, yet variable in strength, with annual mean masses ranging from ~60 to 135 kt (Carn et al., 2017). When these values are compared to ground-based measurements from Tamburello et al. (2014) and this study (extrapolated over a year to facilitate comparison), we find that mean satellite-derived annual SO_2 masses are lower than those extrapolated from ground-based measurements (Fig. 6). These discrepancies could be explained by temporal variability in emissions that are not captured in our discrete ground-based campaigns and/or systematic biases among these measurement techniques. For example, a ground-hugging plume geometry, common at volcanoes with high winds, would hinder detection by satellite and likely cause an underestimation in measured mass. While the accuracy of the satellite observations may require further investigation, temporal variations outside a 1σ standard deviation are evident, suggesting that temporal variations are captured by these observations. Based on these observations, we can conclude that continuous SO_2 emissions of significant quantity have been supplied by Lastarria volcano for at least the past 10 yr and appear to have increased between 2010 and 2015. When we consider the temporal variations between the ground-based SO_2 flux measurements collected in 2012 (884 ± 779 t/d, mean ± standard deviation; Tamburello et al., 2014) and those presented here (604 ± 296 t/d), the relatively high standard deviations and estimated measurement error (50% for SO_2 camera measurements in this study) unfortunately prevent us from identifying temporal changes in SO_2 flux (Fig. 6).

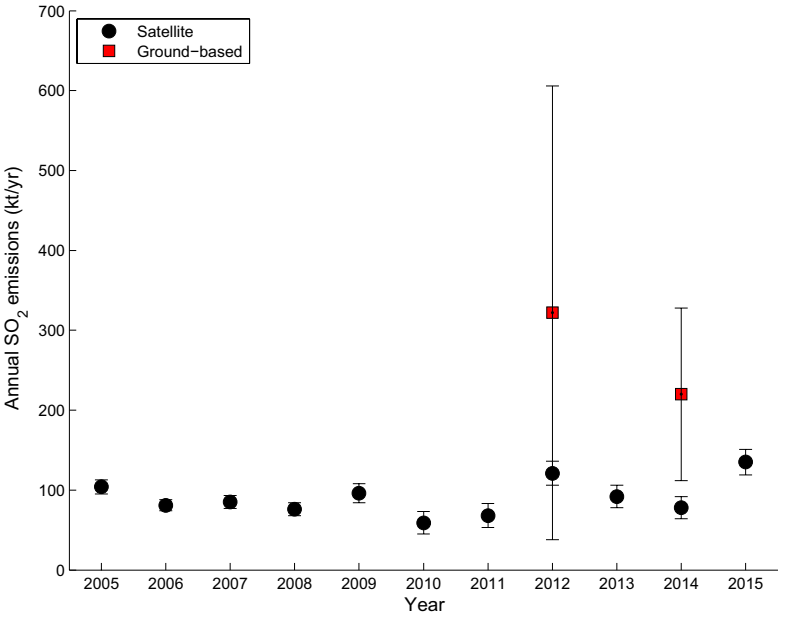

Figure 6. Annual satellite SO_2 masses (kt) (black circles) and extrapolated annual emissions (kt/year) (red squares) based on ground-based measurements for Lastarria volcano. Error bars on both satellite and ground-based SO_2 masses (kt) represent 1σ standard deviation of the mean. Data are from Carn et al. (2017), Tamburello et al. (2014) and this study.

In addition to the somewhat low temporal resolution of our observation set, other factors that can impede interpretations from being made include: (1) spatial variations in the fumarole field, (2) potential biases due to different measurement techniques, and (3) variations in apparent gas composition due to changes in meteorological conditions or regional stresses. Here, by combining direct fumarole samples from a discrete number of fumaroles with bulk plume composition measurements, we eliminate the potential interpretation biases due to spatial variations and technique biases due to using only one of the above methods. Additionally, we consider it unlikely that meteorological changes such as increased precipitation events significantly modified our gas composition measurements in 2014 based on observations by Zimmer et al. (2017). Specifically, those authors found that large precipitation events have only short-term (hours to days) effects on temperature and gas composition at Lastarria, with these parameters quickly returning to their baseline values. No significant precipitation events were observed in the weeks preceding our November 2014 field campaign (Zimmer et al., 2017), such that we do not expect the elevated H_2O in 2014 to be meteoric in origin. We note that isotopic measurements of water from Lastarria fumaroles by Aguilera et al. (2012) showed the water to be largely magmatic in origin, further supporting a magmatic source to Lastarria's water.

Here we evaluate changes in Lastarria's gas composition in recent years and evaluate potential trends with respect to location (i.e., fumarole field), temperature, and sampling method employed (Fig. 7). First, we consider only the normalized concentrations of the following gas compounds: (1) CO_2, total S (S_t), and H_2O; and (2) CO_2, HCl, and S_t. These compositions are presented in ternary diagrams often used to depict the composition of gases from magmatic-hydrothermal systems (e.g., Giggenbach et al., 1990; Symonds et al., 2003; Shinohara et al., 2011; Aiuppa et al., 2015; Fischer and Chiodini, 2015), where clear temporal differences in gas composition can be seen that are well outside of the scatter due to different measurement techniques (Fig. 7). Specifically, in both ternary diagrams, the compositions of gas measured from 2006 to 2009 are dominated by water and/or CO_2, reflecting a more typical hydrothermal gas composition as previously described by Aguilera et al. (2012). Then in 2012 and 2014, the gas composition contains a significant portion of acidic gases (S_t and HCl), relative to the more hydrothermal gases, consistent with shallow degassing magma in the absence of significant scrubbing by hydrothermal water. The scatter in gas composition observed in 2014 is likely due to different sampling and/or analytical techniques, while the apparent clustering observed in both ternary diagrams in 2006–2009 has been attributed to fumarole outlet

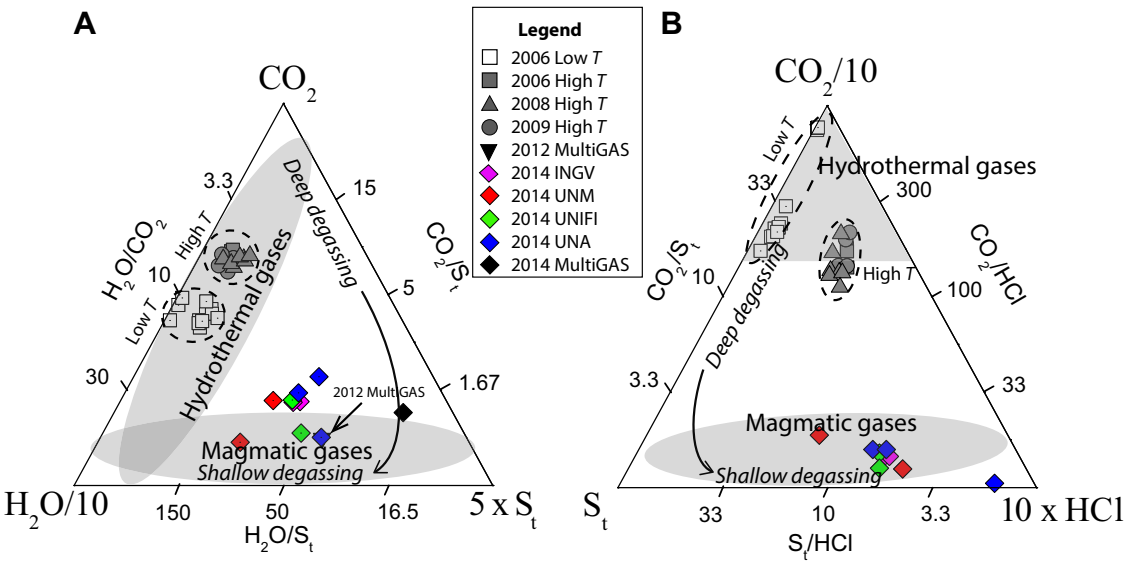

Figure 7. Ternary diagrams depicting Lastarria volcano's normalized gas composition considering H_2O–CO_2–total S (S_t [SO_2 + H_2S]) (A) and S_t-CO_2-HCl (B). Gray and white symbols are samples from 2006-2009 from Aguilera et al. (2012) and represent high- (*T* >120°C) and low-temperature (*T* ≤96°C) fumaroles, respectively. Shaded regions represent compositions typically associated hydrothermal and magmatic gases, while italicized text illustrates approximate compositional changes expected for magma degassing. In both diagrams, a gas composition typical of either (shallow) hydrothermal gases or deep magma is evident in 2006–2009, and a composition typical of shallow magma with minimal hydrothermal scrubbing is observed in 2012–2014. Note that the 2012 multi-component gas analyzer system (MultiGAS) composition from Tamburello et al. (2014) is hidden behind the lower 2014 UNA composition in A, while no MultiGAS composition is available for B because HCl is not measured with that technique. Collection teams: INGV—Istituto Nazionale di Geofisica e Vulcanologia Palermo (Italy); UNM—University of New Mexico (USA); UNIFI—University of Florence (Italy); UNA—Observatorio Vulcanológico y Sismológico de Costa Rica–Universidad Nacional (Costa Rica).

temperature (Aguilera et al., 2012). In Figure 7A, the MultiGAS data show lower relative H_2O content with respect to fumarole sample data, which may be due in part to steam condensation, however further analyses are needed to fully explain the compositional differences observed between these techniques.

In Figure 8, we plot gas ratios to evaluate Lastarria's gas composition measured over the five discrete study periods: May 2006, March 2008, April–June 2009 (Aguilera et al., 2012), November 2012 (Tamburello et al., 2014), and November 2014 (this study). To minimize the influence of shallow processes on gas composition, we plot compositional data from high-temperature (>120 °C) gases only, using the nomenclature of Aguilera et al. (2012). Because no major difference in gas composition was observed between the two fumarole fields during our campaign in 2014 (Table 3), or among these fields in 2006–2009 for the high-temperature fumaroles (Fig. 7), we include measurements from both fields in Figure 8. The composition of fumaroles sampled in 2006, 2008, and 2009 show some scatter, likely due to spatial variations, but the measured gas compositions differ generally from those seen in 2012 and 2014. As we move forward in time from 2006 to 2014, distinct compositional changes can be seen, while some differences due to different sampling techniques are observed. In general, the following changes are observed: (1) the H_2O/CO_2 ratio increases over the five sample periods, with a maximum value observed in 2014; (2) the CO_2/S_t and H_2O/S_t ratios are high between 2006 and 2009 and then low in 2012 and 2014, consistent with enrichment in S gas in recent years; and (3) the S_t/HCl ratios measured by direct sampling appear to be similar throughout the study period, though some temporal variations are observed that may be attributed to different sampling techniques. The simultaneous incremental increase in H_2O/CO_2 along with a decrease in CO_2/S_t and H_2O/S_t from 2006 to 2014 all are consistent with an increase in the proportion of gases emitted with higher solubilities either in the magmatic melt phase and/or water. If we assume that these discrete observations are representative of long-term variations, these changes over time can be explained by four possible scenarios: (1) magma has ascended to relatively shallow depths and has undergone decompression-induced degassing; (2) a stalled, shallow magma body has undergone crystallization-induced degassing; (3) the hydrothermal system has become less voluminous through heating and drying, a decrease in precipitation events, and/or a change in the local stress regime; and/or (4) the hydrothermal system has become increasingly more acidic, such that SO_2 and HCl are no longer being scrubbed as efficiently by water (Symonds et al., 2001; Tamburello et al., 2015; Capaccioni et al., 2016; de Moor et al., 2016b). These scenarios are illustrated in Figure 9.

We next consider each discrete gas observation to determine its consistency with the proposed scenarios. First, an increase in H_2O/CO_2 is consistent with scenarios 1 and 2 (decompression- and crystallization-induced degassing, respectively), but cannot be readily explained by scenarios 3 and 4 (depletion and acidification of hydrothermal water, respectively), where a decrease in H_2O relative to CO_2 and/or no change would be expected. The temporal increase in S_t compared with H_2O and CO_2 over the study period is consistent with all four scenarios, due to the relatively high magma and water solubilities of S species. The fairly consistent S_t/HCl ratios observed from the direct samples in all five campaigns could also be consistent with all four scenarios, though interpretations are less clear due to the complicated solubility behavior of HCl in both

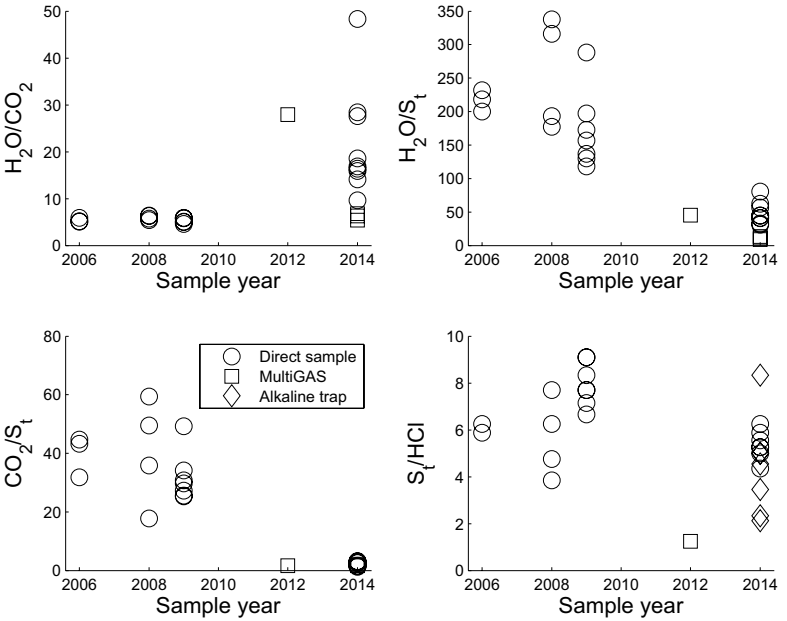

Figure 8. Changes in overall gas composition observed from high-temperature (>120°C) fumarolic emissions from Lastarria volcano from 2006 to 2014. Measurements from both the upper and lower fumarole fields are considered, as well as measurements collected from direct sampling, multi-component gas analyzer system (MultiGAS), and alkaline trap methods. S_t—total S (SO_2 + H_2S).

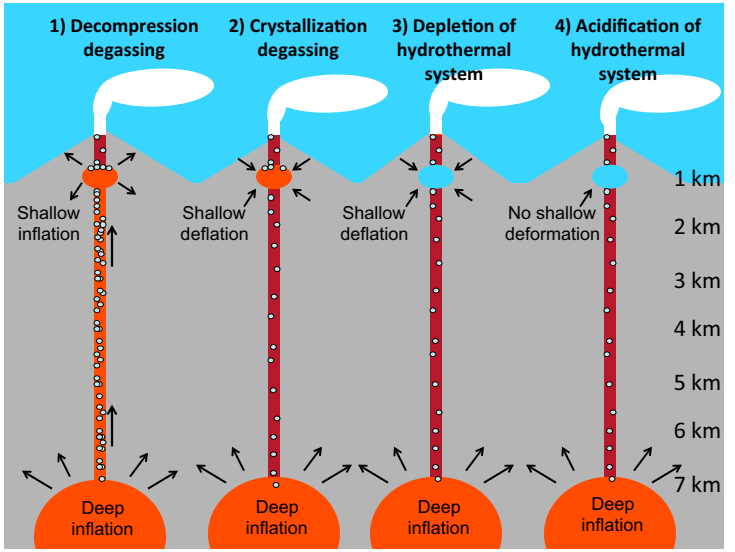

Figure 9. Schematic illustration of the four proposed scenarios to explain the 2014 gas composition at Lastarria volcano and the expected deformation signals associated with these scenarios. See text for details. Approximate depth below the edifice is shown at right. White "bubbles" represent exsolution and transport of volatiles. Orange colors represent volatile-rich magmas, red colors indicate volatile depleted (degassed) magmas, and blue colors represent hydrothermal systems.

water and melts (e.g., Webster et al., 2015). If the temporal variations observed by all measurement techniques are representative of long-term trends and not artifacts of spatial variability and/or differences in measurement technique, than the low S_t/HCl composition observed in 2012 would be most consistent with decompression- or crystallization-induced degassing scenarios based on previous empirical and modeling results of S_t/HCl behavior in volcanic systems (Edmonds et al., 2001; Lesne et al., 2011). Considering these volcanic gas observations, we favor scenarios 1 and 2 as the most likely models to explain subvolcanic conditions at Lastarria volcano during our study period. We next consider existing geophysical constraints to better constrain a subsurface model to explain our observations.

Integration with Geophysical Models

Numerous geophysical studies over the past 20 yr indicate the presence of two shallow crustal inflation sources beneath Lastarria's edifice, presumed to represent magma and magmatic-hydrothermal fluids, respectively. Specifically, InSAR geophysical observations by Pearse and Lundgren (2013) found continued inflation of the ~8-km-depth deformation source beneath the Lazufre region between 2005 and 2010, and again by Henderson et al. (2017) through 2016. To sustain this continuous inflation, we assume that magma has been continuously supplied to this ~8-km-depth crustal storage region from deeper within the crust through 2016. Additionally, InSAR observations by Ruch et al. (2009) indicate inflation of a <1 km source between 2000 and 2008, and seismic tomography results of Spica et al. (2015) identify the presence of low-velocity zones also at <1 km depths below Lastarria between 2008 and 2012. These authors presume that the shallow inflation (Ruch et al., 2009) and spatially coincident low-velocity zone (Spica et al. 2015) represent magmatic volatiles and/or hydrothermal waters, though we argue that shallow magma may be another viable option that would produce the same geophysical signatures. As with the deeper inflation source, we presume that a discrete or continuous supply of magma or volatiles was necessary to produce inflation of the shallow source between 2000 and 2008. No targeted observations of this shallow source are available since 2008, so it is unclear if this shallow source has continued to deform in recent years.

We now consider our gas observations in the context of these geophysical interpretations to constrain a viable subsurface model for Lastarria during

our study period. First, the CO_2-rich composition of Lastarria's high-temperature fumaroles between 2006 and 2009 is consistent with an influx of a deep CO_2-rich magma and a permeable conduit enabling volatiles to reach the surface and outgas in advance of their host magma. The additional changes in high-temperature gas composition observed between April 2009 and November 2014 indicate a change in the magmatic-hydrothermal system during this time. In the absence of updated geophysical data targeting the shallow (<7 km depth) region beneath Lastarria, we simply describe the recent deformation that would be expected for the four scenarios (Fig. 9) if observations were available. Scenario 1 would require continued (since 2009) magma recharge and shallow inflation to explain the measured gas composition and to be consistent with the observed low-velocity zone (Spica et al., 2015) and the pre-2009 deformation signal (Ruch et al., 2009). In this scenario, an increase in SO_2 flux would also be expected, which is not clearly seen in the existing satellite and ground-based data as previously described. Scenario 2 could be explained by shallow inflation prior to 2009, followed by shallow deflation after 2008 as the shallow magma crystallizes and degasses (assuming other parameters are equal). Scenarios 3 and 4 can only be explained if the magmatic gases supplied by the ~8 km magma source condensed and became trapped beneath an impermeable layer to cause the shallow inflation prior to 2009. Because persistent degassing has been observed from Lastarria throughout historical time and quantified with high measured proportions of magmatic gases since 2005 (Carn et al., 2017; Aguilera et al., 2012; Tamburello et al., 2014), a permeable conduit facilitating degassing likely prevails at this volcano, which would make scenarios 3 and 4 less likely. If a change in stress were to cause the sealing of former gas pathways and contribute to gas and/or fluid accumulation in the shallow source, then a decrease in SO_2 emission rates during this time period would be expected, which was also not clearly observed in satellite data by Carn et al. (2017). Considering these factors, we think scenarios 3 and 4 are less likely than the other scenarios to explain observations prior to 2009. Since 2009, a near-surface deflation signal would be expected to support scenario 3, in the case that the hydrothermal system was depleted between 2009 and 2016. No deformation change of the shallow source since 2009 would be expected to support scenario 4, acidification of the hydrothermal system. These interpretations are summarized in Table 5 and Figure 9.

Considering the combined observations in both the gas and deformation data sets, we consider scenarios 1 (decompression-induced degassing) and 2 (crystallization-induced degassing), both involving degassing of a shallow magma source, to be the most likely to explain the recent geochemical and geophysical observations at Lastarria volcano. Additional deformation studies that target shallow depths could help further refine and discriminate between these two scenarios.

Modeled Magma Degassing Depths

We can quantitatively test the validity of scenario 1 by estimating magma degassing depths from the normalized CO_2/H_2O gas composition observed in 2006–2009 and in 2014 using the Lastarria melt composition and volatile solubility trends following the methods of López et al. (2013). The required input parameters to calculate magma degassing depths (assuming degassing due only to decompression) include: initial melt CO_2 and H_2O concentrations; melt composition and temperature at storage depths; degassing pathways (open system versus closed system); and the final gas composition. Due to petrologic analyses of prehistoric Lastarria eruptive products by Stechern et al. (2017), many of these parameters are already constrained or can readily be calculated. Specifically, Stechern et al. (2017) calculated melt H_2O concentrations of up to 6.0 wt% based on amphibole analyses from Lastarria eruptive prod-

TABLE 5. POSSIBLE SUBSURFACE SCENARIOS AT LASTARRIA VOLCANO (NORTHERN CHILE) TO EXPLAIN GEOCHEMICAL AND GEOPHYSICAL OBSERVATIONS

	Scenario 1	Scenario 2	Scenario 3	Scenario 4
Gas observations				
↑ H_2O/CO_2	✔	✔	✖	✖
↓ H_2O/S_t	✔	✔	✔	✔
↓ CO_2/S_t	✔	✔	✔	✔
≈ S_t/HCl	Possible	Possible	Possible	Possible
Persistent SO_2 emissions	✔	✔	✔	✔
Deformation observations				
Deep inflation through 2016	✔	✔	✔	✔
Shallow inflation prior to 2009	✔	✔	Possible	Possible
Shallow low velocity through 2012	✔	✔	✔	✔
Deformation since 2008 required*	Inflation	Deflation	Deflation	No Change

Notes: Checkmark indicates that gas observation is consistent with proposed scenario; X marks indicate that gas observations are not consistent with the proposed scenario. $S_t = SO_2 + H_2S$. Please see Figure 9 for illustration of the proposed scenarios.

*Assumes all other factors remain constant.

ucts and models by Ridolfi et al. (2010) and Ridolfi and Renzulli (2012). They further constrained a rhyolitic melt composition, melt storage pressures of ~200 and 300–550 MPa, and melt temperatures of 840–1060 °C. Using values near the upper bounds calculated by Stechern et al. (2017) of 478 MPa and 1025 °C to represent the deep portion of the crustal storage region, we calculate the amount of CO_2 that could be dissolved in Lastarria melt containing 6 wt% H_2O using VolatileCalc software (Newman and Lowenstern, 2002) to be 1400 ppm. These composition, temperature, and pressure values are used as our initial conditions in the following exercise.

The goal of this exercise is to evaluate how the gas composition changes during decompression ascent from 478 MPa (4780 bars) to the surface. We consider two end-member degassing paths including: (1) open-system degassing where gases readily separate from their host magma and ascend through the conduit and are immediately lost to the system, and (2) closed-system degassing conditions where the gases travel with their host magma and maintain their equilibrium composition with the melt after separation and outgassing. We note that due to the presumed high magma viscosity for a rhyolitic melt, we expect purely open-system degassing conditions to be unlikely at Lastarria volcano and would expect closed-system degassing to dominate until depths at which a permeable conduit is achieved, at which point open-system degassing could commence. In the closed-system degassing case, we consider a concentration of 1 wt% exsolved volatiles (Fig. 10), which is a reasonable value for arc volcanoes (e.g., Edmonds, 2008), and assume that Lastarria's degassing behavior likely represents a combination of the open-system and the closed-system (with 1 wt% exsolved volatiles) end members. Next, we calculate the pressure at which a rhyolitic melt would maintain the observed normalized gas compositions of ~85% H_2O (2006–2009) and ~95% H_2O (2014), with all other factors being equal. These lines of equal composition are referred to as isopleths, and when compared with the magma degassing pathways, can be used to constrain magma degassing depths (Fig. 10). Finally, lines of equal pressure (isobars) for a rhyolitic magma at the assumed 1025 °C temperature can be calculated to enable the intersection of the degassing pathways and gas compositions to be used to estimate magma degassing pressures (i.e., depths). The results of this exercise are shown in Figure 10. The intersection of the ~85 mol% H_2O isopleth (2006–2009) with the open-system and the 1 wt% exsolved gas closed-system degassing pathways occurs at ~270 MPa (~10.5 km) and 170 MPa (6.6 km), respectively. This suggests that based on the observed gas chemistry and our model assumptions, for the time period between 2006 and 2009, the degassing magma beneath Lastarria's edifice likely resided at a mean depth between 10.5 and 6.6 km. This depth range is consistent with the depth of the InSAR-derived mid-crustal storage region throughout this period. The intersection of the ~95% H_2O isopleth (2014) and the open-system and the 1 wt% exsolved gas closed-system degassing pathway occurs at ~230 MPa (~9.0 km) and 50 MPa (1.2 km). This suggests that in 2014 the mean depth of Lastarria's degassing magma likely resided between 9 and 1.2 km. While this most recent range of magma degassing depths is large, it is consistent with magma ascent since 2009. If Lastarria's 2000–2008 near-surface inflation

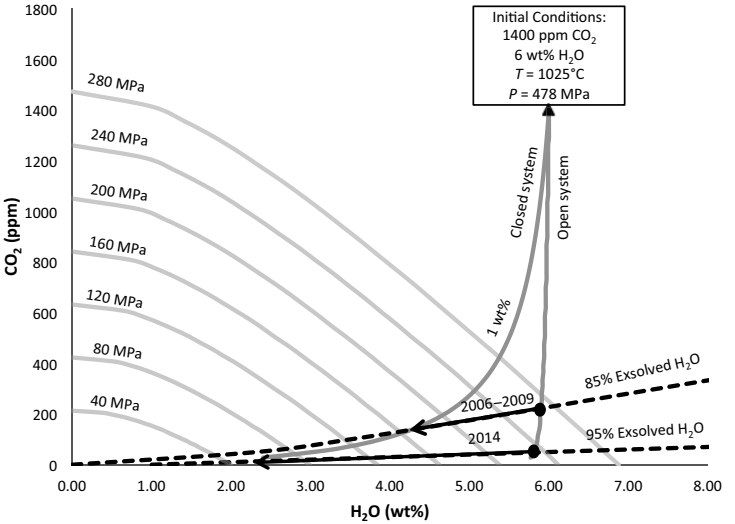

Figure 10. Equilibrium magma degassing behavior modeled for Lastarria volcano's system as a function of dissolved CO_2 (ppm) and H_2O (wt%) concentrations. Initial conditions include a rhyolitic melt with a temperature of ~1025°C containing 1400 ppm CO_2 and 6 wt% H_2O (Stechern et al., 2017). Light gray lines represent lines of equal pressure (isobars). Black dashed lines represent lines of equal composition (isopleths) for volcanic gases measured in 2006–2009 (~85% exsolved H_2O) and 2014 (~95% exsolved H_2O). Dark gray lines represent two degassing scenarios for an ascending magma: (1) open-system degassing, and (2) closed-system degassing containing 1 wt% exsolved fluids. Upper and lower bounds on magma degassing pressures are provided by the intersection of the degassing pathways and the isopleth lines. See text for details. *T*—temperature; *P*—pressure.

source is magma, and has continued to inflate since 2008, then the more-shallow range in magma degassing depths calculated here would be consistent with scenario 1. The relatively high S_t/HCl ratios observed at Lastarria in 2014 are also suggestive of shallow magma (e.g., Edmonds et al., 2001), supporting scenarios 1 and 2, though better constraints on the initial volatile composition from melt inclusion data and improved volatile solubility models that include HCl are needed to test this hypothesis.

Constraints on Volatile Source

Within subduction zone settings, the primary sources of volatiles to arc magmas include: (1) the subducted slab, consisting of altered oceanic crust and overlying marine sediments, (2) the mantle wedge, and (3) the crust. When the isotopic composition of carbon and helium within measured gas samples from arc volcanoes are compared with the end-member compositions of the potential volatile sources, constraints on volatile source can be made (e.g., Sano and Marty, 1995). Specifically, the $\delta^{13}C$-CO_2 composition of mid-ocean

ridge basalt (MORB), which is commonly used as a proxy for upper mantle material, is estimated to be –6.5‰ ± 2‰. The $\delta^{13}C\text{-}CO_2$ composition of carbonate rocks is 0‰, while that of organic sediment is <–20‰ (Sano and Marty, 1995). The $\delta^{13}C\text{-}CO_2$ composition emitted from Lastarria gases in 2014 had a mean value of –2.5‰, which suggests a mixture of carbon sourced primarily from subducted or crustal carbonates and the mantle. The $\delta^{13}C\text{-}CO_2$ composition can be used with the $CO_2/^3He$ composition of the measured gases and the three-component mixing model of Sano and Marty (1995) to calculate the proportion of gases sourced from these three possible end members (Table 2; Fig. 11). Using the average measured CO_2 and He compositions in mole percent from Table 1 along with the R_c/R_a composition measured by CEA (this study) and the known $^3He/^4He$ composition of air, we calculate a $CO_2/^3He$ for 2014 of 2.2×10^{10} (Table 2). This value is within the typical range of arc volcanoes worldwide (Hilton et al., 2002). Using these values, we conduct the three-component mixing calculation and find that the 2014 volcanic gas samples appear to be sourced from 7% mantle-derived volatiles, 87% carbonate-derived volatiles, and 6% organic sediment-derived volatiles (Table 2). This composition has a slightly lower ratio of $CO_2/^3He$ compared with the mean gas samples collected by Aguilera et al. (2012), which are calculated to be sourced from ~2%–7% mantle material, ~89%–91% carbonate, and 4%–9% organic sediment (Fig. 11). The 2014 composition would suggest a slightly greater proportion of mantle-derived volatiles and lower proportion of carbonate volatiles compared to previous years, however spatial variations in individual fumaroles sampled, analytical uncertainties in the measurements, and chemical fractionation during magma degassing (e.g., Barry et al., 2014) can also influence the gas composition and are likely affecting the calculated volatile source proportions. Regardless of these variations, it is clear that Lastarria's volatiles are sourced in large part from carbonate rocks. We note that the calculated volatile-source proportions observed at Lastarria are similar to those of other Central Andean volcanoes including Lascar (Tassi et al., 2009) and Tacora (Capaccioni et al., 2011) volcanoes in northern Chile, suggesting that they have a similar crustal or subducted-slab carbonate source. Because the basement rocks within the Lastarria region are mostly composed of Paleozoic intrusive rocks and Tertiary–Quaternary volcanic rocks (Naranjo, 1992; Naranjo and Cornejo, 1992; Mamani et al., 2008), we can assume that the carbonate and organic volatile signatures are derived from the subducted slab, indicating that the subducted slab is the main volatile source at Lastarria. This interpretation is consistent with the findings of Aguilera et al. (2016), who infer a subducted sediment source for condensed gases sampled from Lastarria in 2014.

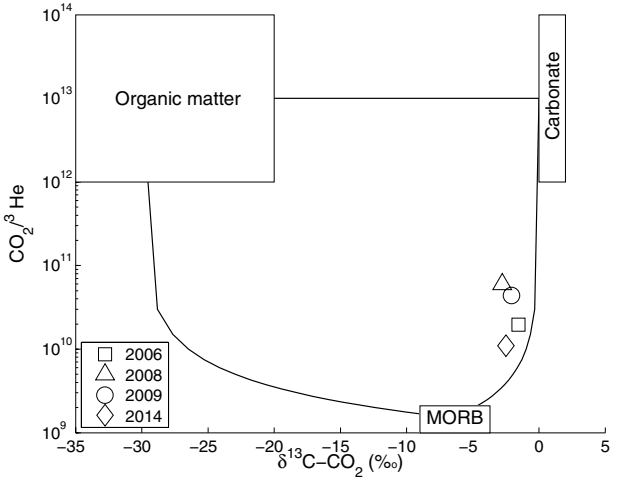

Figure 11. Diagram showing Lastarria volcano's $\delta^{13}C\text{-}CO_2$, which represents the carbon isotopic composition of the sample in comparison with that of the reference standard using standard delta notation, and $CO_2/^3He$ gas composition measured at four discrete times between 2006 and 2014 as a function of mixing among three volatile source end members: (1) upper mantle material (mid-ocean ridge basalt, MORB), (2) carbonates, and (3) organic matter. Black lines depict 2-component mixing curves between two end-member volatile sources. Carbon delta values for the three end members were converted to absolute ratios for the mixing calculations using a $^{13}C/^{12}C$ ratio for Vienna Peedee belemnite (V-PDB) of 1.11802×10^{-2} from Chang and Li (1990). Data are from Aguilera et al. (2012) and this study. See text for details.

Constraints on Total Volatile Flux

Constraints on total volatile flux can be calculated by combining SO_2 flux measurements, diffuse soil CO_2 flux measurements, and gas composition measurements. We assume that our combined average SO_2 flux obtained on 22 November 2014 of 604 ± 296 t/d gives us the most complete and accurate view of Lastarria degassing during our two-day study period. We note that this value is somewhat lower than the average SO_2 flux of 884 ± 779 t/d measured by Tamburello et al. (2014) two years prior (November 2012), however the high standard deviation in the calculated SO_2 fluxes calculated by Tamburello et al. (2014), which exceeds measurement error, indicates high temporal variability in degassing that may not be accurately captured during our brief sample campaigns. Considering this, we calculate a range in possible total volatile fluxes considering the minimum, maximum, and mean SO_2 flux measured (Table 6).

Next we consider the contribution of diffuse CO_2 soil degassing to Lastarria's total volatile flux. Diffuse soil CO_2 degassing measurements were collected over a discrete area near the lower fumarole field to constrain degassing from the sample region. While measurements were collected from this one site only, we assume that diffuse degassing persists at similar rates at other locations around the edifice, acknowledging the limitation of this assumption due to variations in substrate composition and permeability. Previous studies have shown correlations to exist among diffuse degassing, hydrothermal alteration, and elevated surface temperatures at degassing volcanoes (e.g., Chiodini et al., 2001, 2005; Viveiros et al., 2010; Bloomberg et al., 2014). Considering this and the general agreement between regions of higher soil

TABLE 6A. MEASURED GAS RATIOS AND CALCULATED VOLATILE FLUXES FROM LASTARRIA VOLCANO (NORTHERN CHILE): CONSTANT MEAN SO_2 FLUX, RANGE IN COMPOSITION

Composition	Minimum molar ratio*	Mean molar ratio*	Maximum molar ratio*	Gas species	Molar mass (g/mol)	Minimum flux (t/d)	Mean flux (t/d)	Maximum flux (t/d)
				SO_2 (plume)†	64	604	604	604
H_2S/SO_2	0.21	0.46	0.74	H_2S (plume)	34	96	148	338
CO_2/SO_2	1.2	2.8	4.90	CO_2 (plume)	44	710	2035	2900
H_2O/SO_2	10.6	55.2	140	H_2O (plume)	18	2567	9377	33,902
HCl/SO_2	0.15	0.41	0.95	HCl (plume)	36	73.6	141	466
HF/SO_2	0.005	0.008	0.018	HF (plume)	20	1.346	1.5	4.85
				CO_2 (soil measured)		5	5	5
				CO_2 (soil extrapolated)§		95	95	95
				Total volatile flux (CO_2 measured)		4057	12,311	38,221
				Total volatile flux (CO_2 extrapolated)§		4147	12,401	38,311

*Molar ratios are calculated using all direct and in situ measurements collected in 2014 that quantified SO_2.
†SO_2 flux is calculated from the average of all SO_2 flux measurements acquired on 22 November 2014.
§Minimum, mean, and maximum extrapolated areas assume diffuse degassing persists over a ~733,200 m^2 area representing the four fumarole fields. See text for details.

TABLE 6B. MEASURED GAS RATIOS AND CALCULATED VOLATILE FLUXES FROM LASTARRIA VOLCANO (NORTHERN CHILE): RANGE IN SO_2 FLUX, CONSTANT MEAN COMPOSITION

Composition	Mean molar ratio*	Gas species	Molar mass (g/mol)	Minimum flux (t/d)	Mean flux (t/d)	Maximum flux (t/d)
		SO_2 (plume)†	64	171	604	1719
H_2S/SO_2	0.50	H_2S (plume)	34	42	148	420
CO_2/SO_2	2.6	CO_2 (plume)	44	576	2035	5791
H_2O/SO_2	45.6	H_2O (plume)	18	2655	9377	26,687
HCl/SO_2	0.27	HCl (plume)	36	40	141	401
HF/SO_2	0.008	HF (plume)	20	0.4	1.5	4.3
		CO_2 (soil measured)		5	5	5
		CO_2 (soil extrapolated)§		95	95	95
		Total volatile flux (CO_2 measured)		3489	12,311	35,028
		Total volatile flux (CO_2 extrapolated)§		3579	12,401	35,118

*Molar ratios are calculated using all direct and in situ measurements collected in 2014 that quantified SO_2.
†SO_2 flux is calculated from the average of all SO_2 flux measurements acquired on 22 November 2014.
§Minimum, mean and maximum extrapolated areas assume diffuse degassing persists over a ~733,200 m^2 area representing the four fumarole fields. See text for details.

[2]Supplemental Figure S2. Google Earth image of Lastarria's edifice showing regions of hydrothermal mineralization (white to yellow coloring) associated with the main degassing sites. Please visit https://doi.org/10.1130/GES01495.S2 or the full-text article on www.gsapubs.org to view the Supplemental Figure S2.

CO_2 fluxes and soil temperature in the sampled area (excepting the central area where the soil temperature was not measured due to technical problems; Fig. 4, black dots), we conduct the following extrapolation exercise to better constrain the diffuse degassing contribution to Lastarria's total outgassing. First, we identify a region of expected elevated diffuse degassing based on locations where both Google Earth (Digital Globe [http://www.earth.google.com, accessed 5 June 2017]) imagery showed hydrothermal mineralization (Fig. S2[2]) and Advanced Spaceborne Thermal Emission and Reflection Radiometer (ASTER) nighttime thermal infrared data acquired on 19 August 2014 at 03:15 UTC show elevated surface temperatures (Figs. 2 and 12). We ignored regions with apparent elevated thermal temperatures due to differences in emissivity and daytime heating (e.g., the lava flow in the north central part of the image). The selected area is 733,200 m^2 and includes the four fumarole fields outlined by dashed black lines in Figure 12 and by white solid lines in Figure S2 (footnote 2). We note that elevated CO_2 fluxes were measured in our soil survey that do not correspond with elevated thermal temperatures or hydrothermal mineralization as seen in Figure 12, which emphasizes that this remote method is a conservative approximation only. We then assume that diffuse degassing over these selected areas is occurring at the average measured soil CO_2 flux rate of 1.29×10^{-4} t/d/m^2 (measured area shown by solid black rectangle in Fig. 12) to calculate an extrapolated diffuse CO_2 flux of 95 t/d. Acknowledging that our measured flux area represents only a small fraction of the Lastarria edifice, we consider the measured flux of 5 t/d to be the minimum possible diffuse CO_2 flux for Lastarria

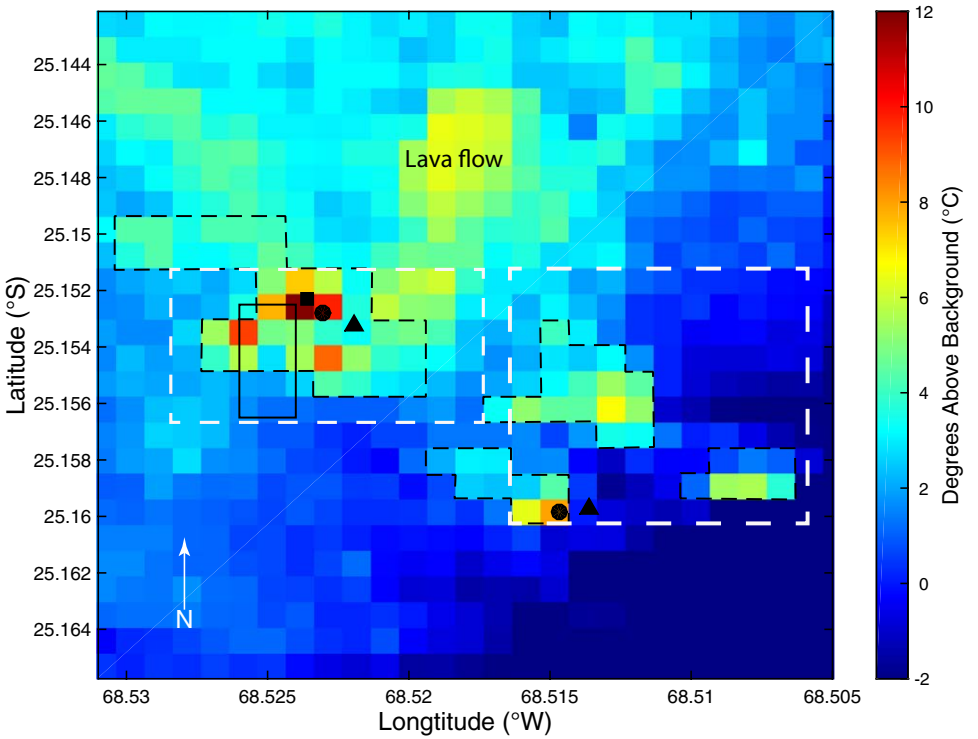

Figure 12. Advanced Spaceborne Thermal Emission and Reflection Radiometer (ASTER) thermal image of Lastarria volcano acquired 19 August 2014. Gas sample measurement locations are shown as squares (multi-component gas analyzer system [MultiGAS] measurements), circles (fumarole samples), triangles (alkaline trap measurements), and a black rectangle (diffuse degassing survey area). Black dashed lines outline the high-temperature regions representing the four main fumarole fields used to extrapolate areas of diffuse degassing. White dashed lines note the regions shown in Figures 2B and 2C. Note that the upper-central portion of the figure shows a thermally elevated area not related to volcanogenic heating. This area is the location of the Lastarria lava flow 4 (<2.4 ka; Naranjo, 1992, 2010) and is labeled in the figure. This area contains the youngest volcanic structures on the complex, including a low-albedo black-colored lava, that have the highest emissivity values. These characteristics enable more thermal energy to be absorbed in these regions during the day and therefore produce a thermally elevated signature in nighttime data.

volcano and consider the extrapolated value calculated here to represent our best estimate of total diffuse degassing, while further acknowledging that a greater flux is also possible. When the extrapolated diffuse soil CO_2 flux is compared to the calculated average plume CO_2 fluxes (Table 6), we calculate that diffuse CO_2 degassing from Lastarria most likely makes up ~6% of total CO_2 degassing (plume degassing + diffuse degassing). This value is similar to what has been observed at other volcanoes with summit plumes including Mount Asama, Japan, which emits ~12% of its total CO_2 diffusively (Morita et al., 2016), and Vulcano, Italy, which releases ~20% of its CO_2 diffusively (Inguaggiato et al., 2012).

Next we calculate an average gas composition using the direct and in situ measurements collected in 2014 (Tables 1, 3) and assume that this result best represents the bulk plume composition from Lastarria. We use the resulting gas ratios with respect to SO_2 and the SO_2 flux of 604 t/d to calculate Lastarria's total flux of the major gas species including H_2O, CO_2, H_2S, HCl, and HF (Table 6). When the calculated plume flux (assuming the average plume composition) and diffuse degassing fluxes are combined, we estimate the most reasonable (average) total degassing flux from Lastarria volcano of ~12,400 t/d or ~4.5 Mt/yr. This estimated total volatile flux agrees very well with that calculated by Tamburello et al. (2014) of ~13,500 t/d, even though the fluxes of individual gas species and plume composition have changed. Acknowledging the differences in gas ratios calculated from the various gas measurement techniques, we also use the minimum and maximum X/SO_2 ratios observed, where X is one of the other primary gas species, to calculate lower and upper bounds of total volatile outgassing from Lastarria's plume during our 2014 field campaign. Through this exercise, we calculate a minimum total volatile flux of ~4150 t/d or ~1.5 Mt/yr, and a maximum total volatile flux of ~38,300 t/d or ~14 Mt/yr. Next, we repeat the total volatile flux calculations using the minimum and maximum SO_2 fluxes measured on 22 November along with the mean gas ratios to better evaluate how variations in SO_2 may influence our total volatile flux calculations. The results are presented in Table 6B and show minimum and maximum total volatile fluxes of ~3600 t/d (~1.3 Mt/yr) and 35,100 t/d (~12.8 Mt/yr), respectively. The highly similar minimum and maximum fluxes calculated using these two methods suggest that the range in possible total volatile fluxes presented in Table 6 well captures the observed variability in outgassing at Lastarria volcano. The wide range in gas composition and flux values observed and used in these calculations highlights the challenges in accurately constraining total degassing from active volcanoes.

CONCLUSIONS

New measurements of volcanic gas composition and flux from Lastarria volcano were acquired during two days in November 2014 and are used to compare and evaluate current gas measurement techniques, present updated constraints on Lastarria's magmatic-hydrothermal system and total degassing budget, and provide further insights into proposed subsurface geophysical models. A qualitative comparison of the various gas sampling and measurement techniques is conducted, and finds good general agreement (within error) among most techniques. The largest variations were seen between direct and in situ (MultiGAS) gas composition measurements, and we recommend that future work aim to resolve the source of these discrepancies. The composition of Lastarria's volcanic gases measured in 2014 was similar to that of 2012, while notably different than measured in 2006–2009. If these observed compositional differences are representative of long-term trends, then a distinct change in Lastarria's magmatic-hydrothermal system likely occurred between 2009 and 2012. The 2014 measured gas composition contained relatively high proportions of H_2O and SO_2 and relatively low proportions of CO_2, and is consistent with degassing of shallow magma. Four possible subsurface scenarios are discussed to explain the apparent temporal variations in measured gas composition, including: (1) decompression-induced degassing due to magma ascent within the shallow crust; (2) crystallization-induced degassing of a stalled magma body; (3) depletion of the hydrothermal system due to heating, changes in local stress, and/or minimal precipitation; and/or (4) acidification of the hydrothermal system. Of these scenarios, options 1 and 2 are most likely due to the observed increase H_2O/CO_2 in 2014 that is not consistent with scenarios 3 and 4. When these scenarios are evaluated in the context of the existing geophysical models, all scenarios are feasible, and would likely produce different shallow deformation signals that could help discriminate the most likely subsurface scenario. We recommend that InSAR analyses be conducted on imagery acquired since 2008 to identify recent deformation changes and constrain which of the four scenarios best describes Lastarria's subsurface system. Lastly, we use the average SO_2 flux calculated on collected on 22 November 2014 of 604 ± 296 t/d, the average plume composition measured through direct sampling and in situ measurements, and extrapolated diffuse degassing measurements to estimate a total degassing budget from Lastarria of ~12,400 t/d, which is similar to that previously estimated in 2012.

ACKNOWLEDGMENTS

The authors would like to thank the organizing committee of the CCVG 12th Gas Workshop who made this project possible, especially Julio Cortés, Cristóbal González, Manuel Inostroza, and Susana Layana for their invaluable support during the field campaign. TL would like to acknowledge funding that supported the collection and analysis of this project from the U.S. National Science Foundation (NSF) PLUTONS project (award 0909254), the NSF GeoPRISMS Program (award 1250148), and the UAF Geophysical Institute. CS and FV would like to acknowledge funding that supported the survey from Fundo Regional da Ciência e Tecnologia (Program M3.3.a from 2014), Governo Regional dos Açores. FV is supported by a post-doctoral grant from Fundação para a Ciência e Tecnologia, Portugal (SFRH/BPD/100032/2014). ALR and ML thank INGV-Palermo colleagues, who provided laboratory support in preparing and analyzing dry gas and alkaline solution samples. NB was supported by a post-doctoral grant from the volcanoes and Atmosphere in Magmatic Open Systems (VAMOS) research unit, University Mainz, Germany. This manuscript was significantly improved by discussions with Matt Pritchard and thorough reviews by Jose Naranjo and two anonymous reviewers.

REFERENCES CITED

Abràmoff, M.D., Magalhães, P.J., and Ram, S.J., 2004, Image processing with ImageJ: Biophotonics International, v. 11, no. 7, p. 36–42.

Aguilera, F., Tassi, F., Darrah, T., Moune, S., and Vaselli, O., 2012, Geochemical model of a magmatic-hydrothermal system at the Lastarria volcano, northern Chile: Bulletin of Volcanology, v. 74, p. 119–134, https://doi.org/10.1007/s00445-011-0489-5.

Aguilera, F., Layana, S., Rodríguez-Díaz, A., González, C., Cortés, J., and Inostroza, M., 2016, Hydrothermal alteration, fumarolic deposits and fluids from Lastarria Volcanic Complex: A multidisciplinary study: Andean Geology, v. 43, p. 166–196, https://doi.org/10.5027/andgeoV43n2-a02.

Aiuppa, A., 2015, Volcanic gas monitoring, *in* Schmidt, A., Fristad, K.E., and Elkins-Tanton, L.T., eds., Volcanism and Global Environmental Change: Cambridge University Press, p. 81–96, https://doi.org/10.1017/CBO9781107415683.009.

Aiuppa, A., Inguaggiato, S., McGonigle, A.J.S., O'Dwyer, M., Oppenheimer, C., Padgett, M.J., Rouwet, D., and Valenza, M., 2005, H_2S fluxes from Mt. Etna, Stromboli, and Vulcano (Italy) and implications for the sulfur budget at volcanoes: Geochimica et Cosmochimica Acta, v. 69, p. 1861–1871, https://doi.org/10.1016/j.gca.2004.09.018.

Aiuppa, A., Moretti, R., Federico, C., Giudice, G., Gurrieri, S., Liuzzo, M., Papale, P., Shinohara, H., and Valenza, M., 2007, Forecasting Etna eruptions by real-time observation of volcanic gas composition: Geology, v. 35, p. 1115–1118, https://doi.org/10.1130/G24149A.1.

Allard, P., Aiuppa, A., Beauducel, F., Gaudin, D., Di Napoli, R., Calabrese, S., Parello, F., Crispi, O., Hammouya, G., and Tamburello, G., 2014, Steam and gas emission rate from La Soufriere volcano, Guadeloupe (Lesser Antilles): Implications for the magmatic supply during degassing unrest: Chemical Geology, v. 384, p. 76–93, https://doi.org/10.1016/j.chemgeo.2014.06.019.

Barazangi, M., and Isacks, B.L., 1976, Spatial distribution of earthquakes and subduction of the Nazca plate beneath South America: Geology, v. 4, p. 686–692, https://doi.org/10.1130/0091-7613(1976)4<686:SDOEAS>2.0.CO;2.

Barazangi, M., and Isacks, B.L., 1979, A comparison of the spatial distribution of mantle earthquakes determined from data produced by local and by telesiesmic networks for the Japan and Aleutian arcs: Bulletin of the Seismological Society of America, v. 69, p. 1763–1770.

Barry, P.H., Hilton, D.R., Füri, E., Halldorsson, S.A., and Grönvold, K., 2014, Carbon isotope and abundance systematics of Icelandic geothermal gases, fluids and subglacial basalts with implications for mantle plume-related CO_2 fluxes: Geochimica et Cosmochimica Acta, v. 134, p. 74–99, https://doi.org/10.1016/j.gca.2014.02.038.

Bloomberg, S., Werner, C., Rissmann, C., Mazot, A., Horton, T., Gravley, D., Kennedy, B., and Oze, C., 2014, Soil CO_2 emissions as a proxy for heat and mass flow assessment, Taupō Volcanic Zone, New Zealand: Geochemistry Geophysics Geosystems, v. 15, p. 4885–4904, https://doi.org/10.1002/2014GC005327.

Businger, S., Huff, R., Pattantyus, A., Horton, K., Sutton, A.J., Elias, T., and Cherubini, T., 2015, Observing and forecasting vog dispersion from Kīlauea volcano, Hawaii: Bulletin of the American Meteorological Society, v. 96, p. 1667–1686, https://doi.org/10.1175/BAMS-D-14-00150.1.

Campion, R., Delgado-Granados, H., and Mori, T., 2015, Image-based correction of the light dilution effect for SO_2 camera measurements: Journal of Volcanology and Geothermal Research, v. 300, p. 48–57, https://doi.org/10.1016/j.jvolgeores.2015.01.004.

Capaccioni, B., Aguilera, F., Tassi, F., Darrah, T., Poreda, R., and Vaselli, O., 2011, Geochemical and isotopic evidences of magmatic inputs in the hydrothermal reservoir feeding the fumarolic discharges of Tacora volcano (northern Chile): Journal of Volcanology and Geothermal Research, v. 208, p. 77–85, https://doi.org/10.1016/j.jvolgeores.2011.09.015.

Capaccioni, B., Rouwet, D., and Tassi, F., 2016, HCl degassing from extremely acidic crater lakes: Preliminary results from experimental determinations and implications for geochemical

monitoring, *in* Ohba, T., Capaccioni, B., and Caudron, C., eds., Geochemistry and Geophysics of Active Volcanic Lakes: Geological Society of London Special Publication 437, p. 97–106, https://doi.org/10.1144/SP437.12.

Cardellini, C., Chiodini, G., and Frondini, F., 2003, Application of stochastic simulation to CO_2 flux from soil: Mapping and quantification of gas release: Journal of Geophysical Research, v. 108, 2425, https://doi.org/10.1029/2002JB002165.

Carn, S.A., Fioletov, V.E., McLinden, C.A., Li, C., and Krotkov, N.A., 2017, A decade of global volcanic SO_2 emissions measured from space: Scientific Reports, v. 7, 44095, https://doi.org/10.1038/srep44095.

Chang, T.L., and Li, W.-J., 1990, A calibrated measurement of the atomic weight of carbon: Chinese Science Bulletin, v. 35, p. 290–296.

Chiodini, G., Cioni, R., Guidi, M., Raco, B., and Marini, L., 1998, Soil CO_2 flux measurements in volcanic and geothermal areas: Applied Geochemistry, v. 13, p. 543–552, https://doi.org/10.1016/S0883-2927(97)00076-0.

Chiodini, G., Frondini, F., Cardellini, C., Granieri, D., Marini, L., and Ventura, G., 2001, CO_2 degassing and energy release at Solfatara volcano, Campi Flegrei, Italy: Journal of Geophysical Research, v. 106, p. 16,213–16,221, https://doi.org/10.1029/2001JB000246.

Chiodini, G., Granieri, D., Avino, R., Caliro, S., Costa, A., and Werner, C., 2005, Carbon dioxide diffuse degassing and estimation of heat release from volcanic and hydrothermal systems: Journal of Geophysical Research, v. 110, B08204, https://doi.org/10.1029/2004JB003542.

de Moor, J.M., Fischer, T.P., Sharp, Z.D., King, P.L., Wilke, M., Botcharnikov, R.E., Cottrell, E., Zelenski, M., Marty, B., Klimm, K., Rivard, C., Ayalew, D., Ramirez, C., and Kelley, K.A., 2013, Sulfur degassing at Erta Ale (Ethiopia) and Masaya (Nicaragua) volcanoes: Implications for degassing processes and oxygen fugacities of basaltic systems: Geochemistry Geophysics Geosystems, v. 14, p. 4076–4108, https://doi.org/10.1002/ggge.20255.

de Moor, J.M., Aiuppa, A., Avard, G., Wehrmann, H., Dunbar, N., Muller, C., Tamburello, G., Giudice, G., Liuzzo, M., Moretti, R., Conde, V., and Galle, B., 2016a, Turmoil at Turrialba Volcano (Costa Rica): Degassing and eruptive processes inferred from high-frequency gas monitoring: Journal of Geophysical Research. Solid Earth, v. 121, p. 5761–5775, https://doi.org/10.1002/2016JB013150.

de Moor, J.M., Aiuppa, A., Pacheco, J., Avard, G., Kern, C., Liuzzo, M., Martínez, M., Giudice, G., and Fischer, T.P., 2016b, Short-period volcanic gas precursors to phreatic eruptions: Insights from Poás Volcano, Costa Rica: Earth and Planetary Science Letters, v. 442, p. 218–227, https://doi.org/10.1016/j.epsl.2016.02.056.

Deutsch, C.V., and Journel, A.G., 1998, GSLIB: Geostatistical Software Library and User's Guide (second edition): New York, Oxford University Press, 369 p.

Edmonds, M., 2008, New geochemical insights into volcanic degassing: Philosophical Transactions of the Royal Society of London A: Mathematical, Physical and Engineering Sciences, v. 366, p. 4559–4579, https://doi.org/10.1098/rsta.2008.0185.

Edmonds, M., Pyle, D., and Oppenheimer, C., 2001, A model for degassing at the Soufrière Hills Volcano, Montserrat, West Indies, based on geochemical data: Earth and Planetary Science Letters, v. 186, p. 159–173, https://doi.org/10.1016/S0012-821X(01)00242-4.

Fischer, T.P., and Chiodini, G., 2015, Volcanic, magmatic and hydrothermal gases, *in* Sigurdsson, H., Houghton, B., McNutt, S., Rymer, H., and Stix, J., eds., The Encyclopedia of Volcanoes (second edition): Elsevier, p. 779–797, https://doi.org/10.1016/B978-0-12-385938-9.00045-6.

Froger, J.-L., Rémy, D., Bonvalot, S., and Legrand, D., 2007, Two scales of inflation at Lastarria–Cordon del Azufre volcanic complex, central Andes, revealed from ASAR-ENVISAT interferometric data: Earth and Planetary Science Letters, v. 255, p. 148–163, https://doi.org/10.1016/j.epsl.2006.12.012.

Galle, B., Johansson, M., Rivera, C., Zhang, Y., Kihlman, M., Kern, C., Lehmann, T., Platt, U., Arellano, S., and Hidalgo, S., 2010, Network for Observation of Volcanic and Atmospheric Change (NOVAC)—A global network for volcanic gas monitoring: Network layout and instrument description: Journal of Geophysical Research, v. 115, D05304, https://doi.org/10.1029/2009JD011823.

Giggenbach, W.F., and Goguel, R.L., 1989, Methods for the collection and analysis of geothermal and volcanic water and gas samples: New Zealand Department of Scientific and Industrial Research, Chemistry Division Report 2387, 53 p.

Giggenbach, W.F., and Matsuo, S., 1991, Evaluation of results from Second and Third IAVCEI Field Workshops on Volcanic Gases, Mt Usu, Japan, and White Island, New Zealand: Applied Geochemistry, v. 6, p. 125–141, https://doi.org/10.1016/0883-2927(91)90024-J.

Giggenbach, W.F., Garcia, N., Londono, A., Rodriguez, L., Rojas, N., and Calvache, M.L., 1990, The chemistry of fumarolic vapor and thermal-spring discharges from the Nevado del Ruiz volcanic-magmatic-hydrothermal system, Colombia: Journal of Volcanology and Geothermal Research, v. 42, p. 13–39, https://doi.org/10.1016/0377-0273(90)90067-P.

Giggenbach, W.F., Tedesco, D., Sulistiyo, Y., Caprai, A., Cioni, R., Favara, R., Fischer, T.P., Hirabayashi, J.-I., Korzhinsky, M., Martini, M., and Menyailov, I., 2001, Evaluation of results from the fourth and fifth IAVCEI field workshops on volcanic gases, Vulcano island, Italy and Java, Indonesia: Journal of Volcanology and Geothermal Research, v. 108, p. 157–172, https://doi.org/10.1016/S0377-0273(00)00283-3.

González-Ferrán, O., 1995, Volcanes de Chile: Santiago, Instituto Geográfico Militar, 639 p.

Henderson, S.T., Delgado, F., Elliott, J., Pritchard, M.E., and Lundgren, P.R., 2017, Decelerating uplift at Lazufre volcanic center, Central Andes, from A.D. 2010 to 2016, and implications for geodetic models: Geosphere, v. 13, p. 1489–1505, https://doi.org/10.1130/GES01441.1.

Hilton, D.R., 1996, The helium and carbon isotope systematics of a continental geothermal system: Results from monitoring studies at Long Valley caldera (California, U.S.A.): Chemical Geology, v. 127, p. 269–295, https://doi.org/10.1016/0009-2541(95)00134-4.

Hilton, D.R., Fischer, T.P., and Marty, B., 2002, Noble gases and volatile recycling at subduction zones: Reviews in Mineralogy and Geochemistry, v. 47, p. 319–370, https://doi.org/10.2138/rmg.2002.47.9.

Horton, K.A., Williams-Jones, G., Garbeil, H., Elias, T., Sutton, A.J., Mouginis-Mark, P., Porter, J.N., and Clegg, S., 2006, Real-time measurement of volcanic SO_2 emissions: Validation of a new UV correlation spectrometer (FLYSPEC): Bulletin of Volcanology, v. 68, p. 323–327, https://doi.org/10.1007/s00445-005-0014-9.

Inguaggiato, S., Mazot, A., Diliberto, I.S., Inguaggiato, C., Madonia, P., Rouwet, D., and Vita, F., 2012, Total CO_2 output from Vulcano island (Aeolian Islands, Italy): Geochemistry Geophysics Geosystems, v. 13, Q02012, https://doi.org/10.1029/2011GC003920.

James, D.E., 1971, Andean crustal and upper mantle structure: Journal of Geophysical Research, v. 76, p. 3246–3271, https://doi.org/10.1029/JB076i014p03246.

Jean-Baptiste, P., Mantisi, F., Dapoigny, A., and Stievenard, M., 1992, Design and performance of a mass spectrometric facility for measuring helium isotopes in natural waters and for low-level tritium determination by the ^{3}He ingrowth method: Applied Radiation and Isotopes, v. 43, p. 881–891, https://doi.org/10.1016/0883-2889(92)90150-D.

Jean-Baptiste, P., Fourré, E., Dapoigny, A., Baumier, D., Baglan, N., and Alanic, G., 2010, ^{3}He mass spectrometry for very low-level measurement of organic tritium in environmental samples: Journal of Environmental Radioactivity, v. 101, p. 185–190, https://doi.org/10.1016/j.jenvrad.2009.10.005.

Kazahaya, R., Mori, T., and Yamamoto, K., 2013, Separate quantification of volcanic gas fluxes from Showa and Minamidake craters at Sakurajima volcano, Japan: Bulletin of the Volcanological Society of Japan, v. 58, p. 183–189, https://doi.org/10.18940/kazan.58.1_183.

Kern, C., Kick, F., Lübcke, P., Vogel, L., Wöhrbach, M., and Platt, U., 2010, Theoretical description of functionality, applications, and limitations of SO_2 cameras for the remote sensing of volcanic plumes: Atmospheric Measurement Techniques, v. 3, p. 733–749, https://doi.org/10.5194/amt-3-733-2010.

Kern, C., Deutschmann, T., Werner, C., Sutton, A.J., Elias, T., and Kelly, P.J., 2012, Improving the accuracy of SO_2 column densities and emission rates obtained from upward-looking UV-spectroscopic measurements of volcanic plumes by taking realistic radiative transfer into account: Journal of Geophysical Research, v. 117, D20302, https://doi.org/10.1029/2012JD017936.

Kern, C., Lübcke, P., Bobrowski, N., Campion, R., Mori, T., Smekens, J.-F., Stebel, K., Tamburello, G., Burton, M., Platt, U., and Prata, F., 2015, Intercomparison of SO_2 camera systems for imaging volcanic gas plumes: Journal of Volcanology and Geothermal Research, v. 300, p. 22–36, https://doi.org/10.1016/j.jvolgeores.2014.08.026.

Lesne, P., Kohn, S.C., Blundy, J., Witham, F., Botcharnikov, R.E., and Behrens, H., 2011, Experimental simulation of closed-system degassing in the system basalt–H_2O–CO_2–S–Cl: Journal of Petrology, v. 52, p. 1737–1762, https://doi.org/10.1093/petrology/egr027.

Levin, I., Münnich, K.O., and Weiss, W., 1980, The effect of anthropogenic CO_2 and ^{14}C sources on the distribution of ^{14}C in the atmosphere: Radiocarbon, v. 22, p. 379–391, https://doi.org/10.1017/S003382220000967X.

Liotta, M., Rizzo, A., Paonita, A., Caracausi, A., and Martelli, M., 2012, Sulfur isotopic compositions of fumarolic and plume gases at Mount Etna (Italy) and inferences on their magmatic source: Geochemistry Geophysics Geosystems, v. 13, Q05015, https://doi.org/10.1029/2012GC004118.

López, T., Ushakov, S., Izbekov, P., Tassi, F., Cahill, C., Neill, O., and Werner, C., 2013, Constraints on magma processes, subsurface conditions, and total volatile flux at Bezymianny Volcano in 2007–2010 from direct and remote volcanic gas measurements: Journal of Volcanology and Geothermal Research, v. 263, p. 92–107, https://doi.org/10.1016/j.jvolgeores.2012.10.015.

Lopez, T., Tassi, F., Aiuppa, A., Galle, B., Rizzo, A.L., Fiebig, F., Capecchiacci, F., Giudice, G., Caliro, S., and Tamburello, G., 2017, Geochemical constraints on volatile sources and subsurface conditions at Mount Martin, Mount Mageik, and Trident Volcanoes, Katmai Volcanic Cluster, Alaska: Journal of Volcanology and Geothermal Research, v. 347, p. 64–81, https://doi.org/10.1016/j.jvolgeores.2017.09.001.

Lucic, G., Stix, J., and Wing, B., 2015, Structural controls on the emission of magmatic carbon dioxide gas, Long Valley Caldera, USA: Journal of Geophysical Research: Solid Earth, v. 120, p. 2262–2278, https://doi.org/10.1002/2014JB011760.

Malowany, K., Stix, J., Van Pelt, A., and Lucic, G., 2015, H_2S interference on CO_2 isotopic measurements using a Picarro G1101-i cavity ring-down spectrometer: Atmospheric Measurement Techniques, v. 8, p. 4075–4082, https://doi.org/10.5194/amt-8-4075-2015.

Mamani, M., Tassara, A., and Wörner, G., 2008, Composition and structural control of crustal domains in the Central Andes: Geochemistry Geophysics Geosystems, v. 9, Q03006, https://doi.org/10.1029/2007GC001925.

Mamyrin, B.A., and Tolstikhin, I.N., 1984, Helium Isotopes in Nature: Amsterdam, Elsevier, Developments in Geochemistry, v. 3, 273 p.

Mitchell, E.C., Fischer, T.P., Hilton, D.R., Hauri, E.H., Shaw, A.M., de Moor, J.M., Sharp, Z.D., and Kazahaya, K., 2010, Nitrogen sources and recycling at subduction zones: Insights from the Izu-Bonin-Mariana arc: Geochemistry Geophysics Geosystems, v. 11, Q02X11, https://doi.org/10.1029/2009GC002783.

Montegrossi, G., Tassi, F., Vaselli, O., Buccianti, A., and Garofalo, K., 2001, Sulfur species in volcanic gases: Analytical Chemistry, v. 73, p. 3709–3715, https://doi.org/10.1021/ac001429b.

Mori, T., Mori, T., Kazahaya, K., Ohwada, M., Hirabayashi, J.I., and Yoshikawa, S., 2006, Effect of UV scattering on SO_2 emission rate measurements: Geophysical Research Letters, v. 33, L17315, https://doi.org/10.1029/2006GL026285.

Morita, M., Mori, T., Kazahaya, R., and Tsuji, H., 2016, Diffuse carbon dioxide emissions from hidden subsurface structures at Asama volcano, Japan: Bulletin of Volcanology, v. 78, no. 17, https://doi.org/10.1007/s00445-016-1008-5.

Naranjo, J.A., 1992, Chemistry and petrological evolution of the Lastarria volcanic complex in the north Chilean Andes: Geological Magazine, v. 129, p. 723–740, https://doi.org/10.1017/S0016756800008451.

Naranjo, J.A., 2010, Geología del Complejo Volcánico Lastarria, Región de Antofagasta: Servicio Nacional de Geología y Minería Carta Geológica de Chile 123, scale 1:25,000.

Naranjo, J.A., and Cornejo, P., 1992, Hoja Salar de la Isla: Servicio Nacional de Geología y Minería Carta Geológica de Chile 72, scale 1:250,000.

Naranjo, J.A., and Puig, A., 1984, Hojas Taltal y Chañaral: Servicio Nacional de Geología y Minería Carta Geológica de Chile 62–63, scale 1:250,000.

Newman, S., and Lowenstern, J.B., 2002, VolatileCalc: A silicate melt–H_2O–CO_2 solution model written in Visual Basic for Excel: Computers & Geosciences, v. 28, p. 597–604, https://doi.org/10.1016/S0098-3004(01)00081-4.

Pearse, J., and Lundgren, P., 2013, Source model of deformation at Lazufre volcanic center, central Andes, constrained by InSAR time series: Geophysical Research Letters, v. 40, p. 1059–1064, https://doi.org/10.1002/grl.50276.

Platt, U., and Stutz, J., 2008, Differential absorption spectroscopy, *in* Platt, U., and Stutz, J., eds., Differential Optical Absorption Spectroscopy: Berlin Heidelberg, Springer, p. 135–174, https://doi.org/10.1007/978-3-540-75776-4_6.

Pritchard, M.E., and Simons, M., 2002, A satellite geodetic survey of large-scale deformation of volcanic centres in the central Andes: Nature, v. 418, p. 167–171, https://doi.org/10.1038/nature00872.

Pritchard, M.E., de Silva, S.L., Michelfelder, G., Zandt, G., McNutt, S.R., Gottsmann, J., West, M.E., Blundy, J., Christensen, D.H., Finnegan, N.J., Minaya, E., Sparks, R.S.J., Sunagua, M., Unsworth, M.J., Alvizuri, C., Comeau, M.J., del Potro, R., Díaz, D., Diez, M., Farrell, A., Henderson, S.T., Jay, J.A., Lopez, T., Legrand, D., Naranjo, J.A., McFarlin, H., Muir, D., Perkins, J.P., Spica, Z., Wilder, A., and Ward, K.M., 2018, Synthesis: PLUTONS: Investigating the relationship between pluton growth and volcanism in the Central Andes: Geosphere, v. 14, doi:10.1130/GES01578.1.

Ridolfi, F., and Renzulli, A., 2012, Calcic amphiboles in calc-alkaline and alkaline magmas: Thermobarometric and chemometric empirical equations valid up to 1,130° C and 2.2 GPa: Contributions to Mineralogy and Petrology, v. 163, p. 877–895, https://doi.org/10.1007/s00410-011-0704-6.

Ridolfi, F., Renzulli, A., and Puerini, M., 2010, Stability and chemical equilibrium of amphibole in calc-alkaline magmas: An overview, new thermobarometric formulations and application to subduction-related volcanoes: Contributions to Mineralogy and Petrology, v. 160, p. 45–66, https://doi.org/10.1007/s00410-009-0465-7.

Rizzo, A.L., Caracausi, A., Liotta, M., Paonita, A., Barnes, J.D., Corsaro, R.A., and Martelli, M., 2013, Chlorine isotope composition of volcanic gases and rocks at Mount Etna (Italy) and inferences on the local mantle source: Earth and Planetary Science Letters, v. 371, p. 134–142, https://doi.org/10.1016/j.epsl.2013.04.004.

Roberts, L.R., and McKee, H.C., 1959, Evaluation of absorption sampling devices: Journal of the Air Pollution Control Association, v. 9, p. 51–53, https://doi.org/10.1080/00022470.1959.10467873.

Ruch, J., Manconi, A., Zeni, G., Solaro, G., Pepe, A., Shirzaei, M., Walter, T.R., and Lanari, R., 2009, Stress transfer in the Lazufre volcanic area, central Andes: Geophysical Research Letters, v. 36, L22303, https://doi.org/10.1029/2009GL041276.

Sano, Y., and Marty, B., 1995, Origin of carbon in fumarolic gas from island arcs: Chemical Geology, v. 119, p. 265–274, https://doi.org/10.1016/0009-2541(94)00097-R.

Shinohara, H., Matsushima, N., Kazahaya, K., and Ohwada, M., 2011, Magma-hydrothermal system interaction inferred from volcanic gas measurements obtained during 2003–2008 at Meakandake volcano, Hokkaido, Japan: Bulletin of Volcanology, v. 73, p. 409–421, https://doi.org/10.1007/s00445-011-0463-2.

Sortino, F., Inguaggiato, S., and Francofonte, S., 1991, Determination of HF, HCl, and total sulphur in fumarolic fluids by ion chromatography: Acta Vulcanologica, v. 1, p. 89–91.

Spica, Z., Legrand, D., Iglesias, A., Walter, T.R., Heimann, S., Dahm, T., Froger, J.-L., Rémy, D., Bonvalot, S., West, M., and Pardo, M., 2015, Hydrothermal and magmatic reservoirs at Lazufre volcanic area, revealed by a high-resolution seismic noise tomography: Earth and Planetary Science Letters, v. 421, p. 27–38, https://doi.org/10.1016/j.epsl.2015.03.042.

Stechern, A., Just, T., Holtz, F., Namur, O., and Blume-Oeste, M., 2017, Decoding magma plumbing and geochemical evolution beneath the Lastarria volcanic complex (Northern Chile): Evidence for multiple magma storage regions: Journal of Volcanology and Geothermal Research, v. 338, p. 25–45, https://doi.org/10.1016/j.jvolgeores.2017.03.018.

Symonds, R.B., Gerlach, T.M., and Reed, M.H., 2001, Magmatic gas scrubbing: Implications for volcano monitoring: Journal of Volcanology and Geothermal Research, v. 108, p. 303–341, https://doi.org/10.1016/S0377-0273(00)00292-4.

Symonds, R.B., Janik, C.J., Evans, W.C., Ritchie, B.E., Counce, D., Poreda, R.J., and Iven, M., 2003, Scrubbing masks magmatic degassing during repose at Cascade-Range and Aleutian-Arc volcanoes: U.S. Geological Survey Open-File Report 03-435, 22 p.

Taddeucci, J., Scarlato, P., Capponi, A., Del Bello, E., Cimarelli, C., Palladino, D.M., and Kueppers, U., 2012, High-speed imaging of Strombolian explosions: The ejection velocity of pyroclasts: Geophysical Research Letters, v. 39, L02301, https://doi.org/10.1029/2011GL050404.

Tamburello, G., 2015, Ratiocalc: Software for processing data from multicomponent volcanic gas analyzers: Computers & Geosciences, v. 82, p. 63–67, https://doi.org/10.1016/j.cageo.2015.05.004.

Tamburello, G., Aiuppa, A., McGonigle, A.J.S., Allard, P., Cannata, A., Giudice, G., Kantzas, E.P., and Pering, T.D., 2013, Periodic volcanic degassing behavior: The Mount Etna example: Geophysical Research Letters, v. 40, p. 4818–4822, https://doi.org/10.1002/grl.50924.

Tamburello, G., Hansteen, T.H., Bredemeyer, S., Aiuppa, A., and Tassi, F., 2014, Gas emissions from five volcanoes in northern Chile and implications for the volatiles budget of the Central Volcanic Zone: Geophysical Research Letters, v. 41, p. 4961–4969, https://doi.org/10.1002/2014GL060653.

Tamburello, G., Agusto, M., Caselli, A., Tassi, F., Vaselli, O., Calabrese, S., Rouwet, D., Capaccioni, B., Di Napoli, R., Cardellini, C., Chiodini, G., Bitetto, M., Brusca, L., Bellomo, S., and Aiuppa, A., 2015, Intense magmatic degassing through the lake of Copahue volcano, 2013–2014: Journal of Geophysical Research: Solid Earth, v. 120, p. 6071–6084, https://doi.org/10.1002/2015JB012160.

Tassi, F., Aguilera, F., Vaselli, O., Medina, E., Tedesco, D., Delgado Huertas, A., Poreda, R., and Kojima, S., 2009, The magmatic- and hydrothermal-dominated fumarolic system at the Active Crater of Lascar volcano, northern Chile: Bulletin of Volcanology, v. 71, p. 171–183, https://doi.org/10.1007/s00445-008-0216-z.

Vaselli, O., Tassi, F., Montegrossi, G., Capaccioni, B., and Giannini, L., 2006, Sampling and analysis of fumarolic gases: Acta Vulcanologica, v. 18, p. 65–76.

Viveiros, F., Cardellini, C., Ferreira, T., Caliro, S., Chiodini, G., and Silva, C., 2010, Soil CO_2 emissions at Furnas volcano, São Miguel Island, Azores archipelago: Volcano monitoring perspectives, geomorphologic studies, and land use planning application: Journal of Geophysical Research, v. 115, B12208, https://doi.org/10.1029/2010JB007555.

Webster, J.D., Vetere, F., Botcharnikov, R.E., Goldoff, B., McBirney, A., and Doherty, A.L., 2015, Experimental and modeled chlorine solubilities in aluminosilicate melts at 1 to 7000 bars and 700 to 1250°C: Applications to magmas of Augustine Volcano, Alaska: The American Mineralogist, v. 100, no. 2–3, p. 522–535, https://doi.org/10.2138/am-2015-5014.

Wittmer, J., Bobrowski, N., Liotta, M., Giuffrida, G., Calabrese, S., and Platt, U., 2014, Active alkaline traps to determine acidic-gas ratios in volcanic plumes: Sampling techniques and analytical methods: Geochemistry Geophysics Geosystems, v. 15, p. 2797–2820, https://doi.org/10.1002/2013GC005133.

Zhang, Y., and Johansson, M., 2009, Mobile-DOAS software: Gothenburg, Sweden, Chalmers University of Technology, Optical Remote Sensing Group.

Zimmer, M., Walter, T.R., Kujawa, C., Gaete, A., and Franco-Marín, L., 2017, Thermal and gas dynamic investigations at Lastarria volcano, Northern Chile: The influence of precipitation and atmospheric pressure on the fumarole temperature and the gas velocity: Journal of Volcanology and Geothermal Research, v. 346, p. 134–140, https://doi.org/10.1016/j.jvolgeores.2017.03.013.